How EGF and IGF1 activate their receptors: mechanisms of autoinhibition and activation

by

Patrick Byrne

A dissertation submitted to Johns Hopkins University in conformity with the requirements for the degree of Doctor of Philosophy

Baltimore, Maryland

July 2016

Abstract

Growth factors and their cell-surface receptors play important roles in metazoan signaling, contributing to both normal development and the progression of disease. The past few decades have witnessed considerable advancement in our understanding of how one class of transmembrane receptors, the receptor tyrosine kinases (RTKs), transduce signals across the membrane. Biochemical investigation of isolated components of the receptors, as well as studies of receptors expressed in cultured cells, have revealed key features of the mechanisms that regulate receptor autoinhibition and ligand-induced activation. With few exceptions, all RTKs are composed of an extracellular ligand-binding domain, a single transmembrane alpha-helix, and an intracellular tyrosine kinase domain. Receptors exist on the plasma membrane in equilibrium between monomers and oligomers, and ligand binding to the extracellular domains promotes the formation of active oligomers or induces conformational rearrangement within ligand-independent oligomers, or both. Once activated, the tyrosine kinase domains phosphorylate their receptor dimer partners as well as downstream cytosolic substrates, thus propagating transduction of the signal.

Despite this considerable progress, the models derived from biochemical studies of purified receptor components fail to explain important features of receptor function in cells, such as (i) the existence of negative cooperativity in receptor-ligand binding and (ii) the existence of ligand-independent oligomers (Lemmon, 2009) (Endres, et al., 2014). In particular, the relationship between dimer formation and activation remains unclear.

Dimerization is required for receptors to become activated, but dimerization itself is not sufficient to fully activate the kinase domains.

Much of the uncertainty surrounding receptor function may arise due to a dearth of structural and biochemical studies of receptors embedded in a native bilayer environment. To address these issues, we employed a variety of biochemical and biophysical methods to investigate the relationship between receptor dimer formation and receptor activation in two types of RTKs: the epidermal growth factor receptors (EGFR/ErbB) and the insulin/insulin-like growth factor receptor (IR/IGF1R). Biochemical studies of receptor function in cultured cells allowed us to compare the signaling characteristics of wild-type and genetically-modified receptors. Mutational analysis revealed regions of receptor that are important for both receptor autoinhibition and kinase activation. We then used quantitative imaging confocal FRET microscopy (QI-FRET) to investigate the relationship between receptor oligomerization and receptor activation. For both ErbBs and IGF1R, we observed that isolated transmembrane domains tend to form strong dimers, and that the extracellular domains impede intrinsic TM domain interactions. Ligand binding relieves ECD autoinhibition, allowing for TM association.

For the ErbB family, our results indicate that dimer formation depends upon receptor concentration in the membrane, with the intracellular domain promoting dimer formation in the absence of ligand. Increased levels of ErbB1 cell surface expression correlate with low levels of ligand-independent kinase activity. Moreover, the expression threshold at which ligand-independent dimerization begins agrees closely with the 2D-

dimerization constant determined from FRET experiments. Unliganded EGFR dimers therefore form according the law of mass action, and are likely populated by a mixture of active and inactive states. The receptor thus follows one of two possible mechanisms upon ligand binding, depending on the receptor surface density: a switch from inactive monomers to active dimers in the low expression regime, and a transition from inactive to active dimers in the high expression regime. Taken together, these studies have identified transmembrane separation as an important determinant of RTK dimer activity, and reinforce the need for biophysical measurements of receptors in the native bilayer environment.

Acknowledgements

I owe a large debt of gratitude to Kalina Hristova and all the members of her laboratory, in particular Sarvenaz Sarabipour, Chris King, and Nuala Del Piccolo. Their expertise in all things related to fluorescence, microscopy and membrane biophysics enabled much of the research presented in this work. I am certain that I could not have done it without them.

To my numerous friends and colleagues in the department of Biophysics and Biophysical Chemistry, as well as the Program in Molecular Biophysics, I owe many thanks for their constant support and advice in matters both scientific and social: a finer group of co-workers I have yet to meet.

Many thanks to my advisor Dan Leahy, for allowing me the freedom to pursue a research project that required extensive collaboration and time spent outside his laboratory. I owe much of my improvement and development as a scientist to his lucid observations, keen suggestions, and easygoing manner. To my Leahy lab-mates, in particular Jennifer Kavran, Matt Ward, Lily Raines and Jackie McCabe: thank you. Each of you pushed me to become a better scientist in one way or another, and for that I am ever grateful.

Last, but not least, all my thanks and gratitude to my parents and siblings for their love and support during the last six years, and to my wife Maria, who went with me every step of the way.

Table of Contents

List of Figures and Tables

Chapter 1. A single ligand is sufficient to activate EGFR dimers

Note to reader: This chapter comprises excerpts from the following reference: (Liu, et al., 2012). It has been edited for clarity.

Acknowledgements

This work was performed in collaboration with Ping Liu, Tom Cleveland, Patti Longo, and Samuel Bouyain in the Leahy Lab. Thanks for their work in preparing the cell lines used for study and their advice in troubleshooting technical issues.

Abstract

Crystal structures of human epidermal growth factor receptor (EGFR) with bound ligand revealed symmetric, doubly ligated receptor dimers thought to represent physiologically active states. Such complexes fail to rationalize negative cooperativity of epidermal growth factor (EGF) binding to EGFR and the behavior of the ligandless EGFR homolog ErbB2/HER2, however. We report cell-based assays that provide evidence for active, singly ligated dimers of human EGFR and its homolog, ErbB4/HER4.

Introduction

Human epidermal growth factor receptor (EGFR) and its homologs, known as ErbBs or HERs, are essential receptor tyrosine kinases that mediate cell proliferation and

differentiation during animal development and are the targets of multiple cancer therapies (Burgess, 2008). EGFR is the archetype of single-pass membrane-spanning receptors thought to transmit signals by ligand-induced dimerization (Heldin, 1995) (Yarden & Schlessinger, 1987), and structural studies show that ligand binding to human EGFR promotes rearrangement of its four extracellular domains from a tethered to an extended conformation in which a loop, termed the dimerization arm, becomes exposed and mediates formation of symmetric receptor dimers (Burgess, 2003) (Fig 1.1A). At odds with a ligand-induced dimerization model of EGFR signaling, however, are recent studies showing dimers of human EGFR in the absence of ligand (Chung, et al., 2010) (Gadella & Jovin, 1995) (Moriki, et al., 2001) (Sako, et al., 2000) as well as negative cooperativity when epidermal growth factor (EGF) binds to EGFR (Macdonald & Pike, 2008). Curiously, the single *Drosophila* EGFR homolog adopts an extended conformation in the absence of ligand and forms asymmetric receptor dimers with a single high-affinity ligand bound (Alvarado, et al., 2010) (Zhang, et al., 2010), suggesting different mechanisms may regulate EGFR activation in *Drosophila* and humans.

We report here evidence for active, singly ligated homodimers of human EGFR and its homolog, ErbB4. These results compel reappraisal of canonical views of ligand-induced dimerization and show that several previously anomalous properties of human EGFR and its homologs represent vertebrate innovations on a core signaling mechanism present in invertebrates.

Results and Discussion

We reasoned that if singly ligated dimers of human EGFR exist as implied by negative cooperativity (Macdonald & Pike, 2008), an EGFR variant incapable of binding ligand may remain able to participate in signaling dimers. To test this idea, we introduced debilitating amino-acid substitutions into the ligand-binding site of one EGFR variant and the kinase active site of another. These variants show negligible ligand-dependent phosphorylation when expressed individually in CHO cells, but co-expression restores phosphorylation in response to ligand as judged by both general and specific anti-phosphotyrosine antibodies (Fig. 1.1B and Table 1.1). The simplest explanation for this observation is that ligand-binding deficient receptors are able to pair with kinase-deficient receptors to form active, singly ligated EGFR dimers. Similar results were obtained for ErbB4/HER4 (Fig. 1.1C). Amino-acid substitutions in the ErbB4 dimerization arm in the context of either ligand-binding or kinase-activity deficient ErbB4 variants eliminates responsiveness when co-transfected, implicating dimerization arms from both partners in formation of singly ligated ErbB4 dimers. Participation of unliganded ErbBs in a signaling dimer despite burial of the dimerization arm in the tethered conformation likely reflects favorable energetics of the inter-receptor dimer interface relative to the tethered state within a preformed dimer.

An essential feature of EGFR activation is an asymmetric dimer of EGFR kinase domains in which the C-terminal region of a “donor” kinase contacts the N-terminal region of an “acceptor” kinase and stimulates it (Zhang, et al., 2010) (Fig. 1.1A), and the question arises whether the extracellular asymmetry of singly ligated EGFR dimers is

coupled to this intracellular asymmetry. The ability of ligand-binding deficient EGFR to be activated by kinase-dead EGFR demonstrates that unliganded EGFRs can function as the acceptor kinase (Fig. 1.1B). To determine if ligand-binding deficient EGFR can function as a donor kinase, debilitating amino-acid substitutions were simultaneously introduced into the ligand-binding and kinase active sites of one EGFR and into the kinase donor site of another EGFR. Neither variant showed ligand-dependent phosphorylation when expressed on its own, but weak, ligand-dependent phosphorylation was observed when co-expressed (Fig. 1.1B). Similar results were obtained for ErbB4 (Fig. 1.1C). This observation suggests that unliganded EGFRs can serve as both a donor and an acceptor kinase and that extracellular asymmetry is not absolutely coupled to intracellular asymmetry, consistent with studies suggesting a loose linkage between ligand binding and kinase activation (Lu, 2010). A recent report using a luciferase fragment complementation assay showed that normal activation of EGFR/ErbB2 heterodimers required the EGFR kinase to be active, suggesting that the liganded partner (EGFR) could initially only function as an acceptor kinase and that extra- and intracellular asymmetry are coupled (Macdonald-Obermann, et al., 2012). In this case the intracellular kinases differ (vs. EGFR or ErbB4 homodimers), which may contribute to additional stabilization of the EGFR kinase in the acceptor role in the absence of phosphorylation. It will be interesting to determine if this is indeed the case or whether other factors underlie this apparent difference. The sites of all tested amino-acid substitutions are listed in Table 1.1. None of these sites impaired cell surface expression as judged by cell-surface biotinylation, and EGFR expression levels were estimated by

Western blot (Table 1.2, Fig. 1.2). Curiously, an original ligand-binding mutation introduced in EGFR, D355R, failed to express on the cell surface unless co-transfected with kinase-deficient EGFR. This observation suggests that EGFR molecules interact early in biogenesis and that this interaction can rescue otherwise nonviable forms of EGFR.

Participation of unliganded ErbBs in active signaling complexes prompts reassessment of the role of the tethered conformation, which was first interpreted as keeping ErbBs "off" in the absence of ligand (Burgess, 2003) (Cho & Leahy, 2002) (Ferguson, et al., 2003). It is now apparent that the straight conformation of domain II is sufficient for this purpose, as evidenced by the absence of a tethered conformation in *Drosophila* EGFR and the failure of tether mutations in human EGFR to result in receptor activation (Alvarado, et al., 2010) (Mattoon, et al., 2004) (Walker, et al., 2004). In an organism with multiple EGFR homologs, however, the ability of an unliganded ErbB to participate in a signaling complex means that ligand binding to any ErbB could activate all coexpressed ErbBs. Such promiscuous activation is observed for ErbB2/HER2, for example, which is the only vertebrate ErbB not to adopt a tethered conformation. An additional inhibitory mechanism was thus needed to prevent indiscriminate ErbB responses to individual ligands in species with multiple ErbB homologs. By precluding unliganded EGFR, ErbB3, or ErbB4 from pairing with liganded forms of other ErbBs, the tethered conformation fulfills this role and likely facilitated diversification of ErbB function. The tethered conformation of human EGFR (Ferguson, et al., 2003), ErbB3 (Cho & Leahy, 2002), and ErbB4 (Bouyain, et al., 2005) and the

fixed, ligandless conformation of ErbB2 (Cho, et al., 2003) (Garrett, et al., 2003) thus appear to have arisen following the appearance of multiple ErbB homologs as elaborations on the core signaling mechanism present in *Drosophila* EGFR. As tethered ErbBs appear able to convert to a signaling competent extended-straight conformation when dimerized with a liganded partner, which ErbB dimers form in the absence of ligand will govern the nature of ErbB responses and is an important avenue for future investigation. The stability of doubly-ligated ErbBs may have arisen to allow heterodimerization of ErbBs when ligands for both are present.

ErbBs have evolved many mechanisms to safeguard and modulate their potent activity. The presence of inactive, singly ligated, and doubly ligated human ErbB dimers confers several advantages over a ligand-induced dimerization activation mechanism. Inactive dimers present a barrier to activation through random dimerization, and the presence of singly and doubly ligated dimers furnishes a mechanism to tune responses to different concentrations or affinities of ligands (Alvarado, et al., 2010). The results presented here show how specific intra- and intermolecular conformations combine to govern ErbB activity and lead to a unifying model of ErbB activation that rationalizes previously puzzling properties of EGFR and its homologs.

Materials and Methods

Generation of ErbB-expressing Cell Lines

Genes encoding ErbB mutants were generated by QuikChange mutagenesis (Stratagene) using PfuTurbo AD (Agilent) and sequenced. Variant ErbB genes were then

subcloned with their native signal sequences into pSSX, a version of pSGHV0 modified to eliminate the growth hormone tag and add C-terminal Flag or HA tags (Leahy, et al., 2000). CHO-S cells (Invitrogen) were maintained in adherent culture in DMEM:F12 supplemented with 5% FBS. Stably transfected cell lines were created using FuGENE (Roche) according to manufacturer's instructions. Cells were cotransfected with a total of 1 μg DNA per ml culture and 0.1 μg per ml of pCDNA 3.1 (Invitrogen), which contains the neomycin resistance gene. After 24 hours, fresh medium containing 1 mg/ml G418 was added, and the cells fed every three days until colonies appeared. Colonies were picked, expanded, and screened for ErbB expression by Western using the appropriate tag antibody.

Antibodies used for immunoprecipitation or Western detection were Flag-M2 (Sigma), 3F10 anti-HA (Roche), anti-EGFR (Santa Cruz sc-71033), anti-EGFR pY1068 (Abcam EP774Y), anti-ErbB4 (Santa Cruz sc-283), and 4G10 antiphosphotyrosine (Millipore). The number of receptors per cell was estimated by comparison of anti-EGFR band intensities of cell lysates compared to intensities of known amounts of purified tEGFR (Qiu, et al., 2009); cell lines with approximately equal expression of the ErbB variants were chosen for stimulation assays.

ErbB Activity Assays

ErbB-expressing cell lines were plated in 2 wells of a six-well plate at 0.2×10^6 cells per well and grown 24 hr. On the day of the assay, cells were washed three times with 2 ml Ham's F12 supplemented with 1 mg/ml BSA, then serum-starved for at least 3 hours at 37 °C in the same medium. EGF or Nrg1β was added to one of the two

wells at a final concentration of 100 ng ml^{-1}, and the plates incubated at 37 °C for 5 minutes. The wells were then washed once with ice-cold phosphate-buffered saline, and 250 µl of RIPA buffer (50 mM Tris pH 8, 150 mM NaCl, 1% NP-40, 0.5% sodium deoxycholate, and 0.1% SDS) supplemented with 1 mM activated Na_3VO_4, 1 mM PMSF, and Benzonase nuclease (Sigma) was added directly to the wells. The cells were allowed to lyse for 30 minutes with gentle rocking, and the appropriate antibody was added to the lysate (using 0.5 µg/ml for anti-Flag and 0.1 µg/ml for anti-HA). Lysates were next added directly to 20 µl Protein G Sepharose 4 Fast Flow (GE), and allowed to bind overnight at 4 °C. Finally, beads were washed 3 times with 1 ml of RIPA buffer supplemented with 1 mM activated Na_3VO_4 and eluted by adding 20 µl of 5× SDS-PAGE loading buffer containing 10% fresh β-mercaptoethanol and incubating for 30 minutes at room temperature. Eluted proteins were separated on 4% to 20% Tris-Glycine SDS-PAGE gels (Invitrogen), transferred to PVDF membranes, and probed with the antiphosphotyrosine antibody 4G10. A portion of crude lysate was reserved, run separately, and probed with antibodies against HA, Flag, EGFR, or ErbB4 to assess total receptor expression.

Figure 1.1 Evidence for singly ligated ErbB signaling dimers

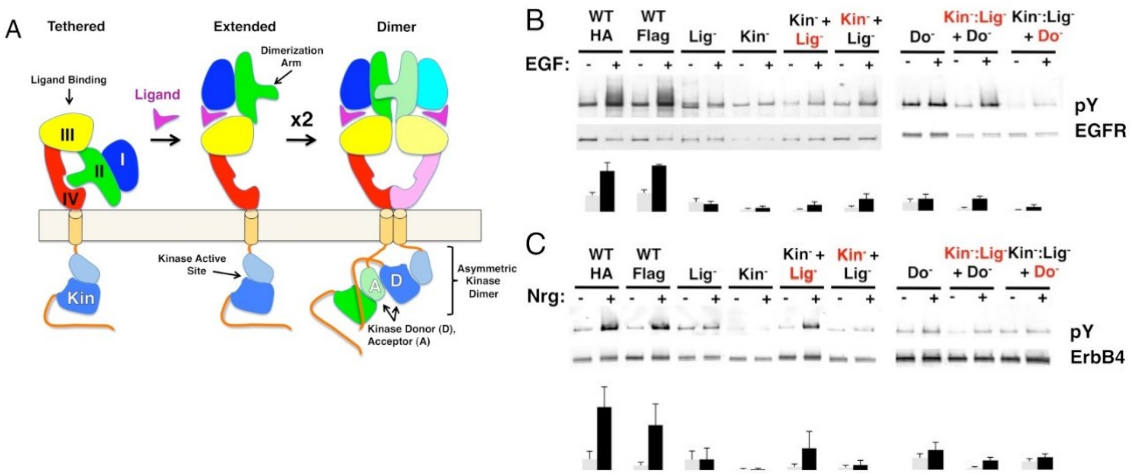

Figure 1.1. Evidence for singly ligated ErbB signaling dimers. (*A*) Schematic diagram showing tethered, extended, and dimeric conformations of EGFR with sites of function-targeting mutations indicated. (*B*) Anti-phosphotyrosine and anti-EGFR Western blots of tagged full-length EGFR immunoprecipitated from stably transfected CHO cells. Wild-type (WT) EGFR was tagged with either hemagglutinin (HA) or Flag peptides, EGFR bearing an inactivating mutation in its kinase active site (Kin$^-$) was tagged with HA, and EGFR bearing a mutation in its ligand-binding site (Lig$^-$) was tagged with Flag. Mutation in the Kinase donor site (Do$^-$) and combination of the Kinase$^-$ and Ligand-targeting mutations on a single EGFR (Kin$^-$: Lig$^-$) were also tested. Serum-starved cells were either untreated (−) or treated (+) with EGF for 5 minutes. Each WT or mutant EGFR was transfected singly; the Kin$^-$ and Lig$^-$ variant EGFRs were co-transfected as were the (Kin$^-$: Lig$^-$) and (Do$^-$) variants. When co-transfected, the tag used for immunoprecipitation prior to Western blotting is indicated in red. (*C*) Similar experiments using ErbB4 and its ligand Neuregulin 1β (Nrg) are shown. The lanes shown were run on the same gel, but

rearranged electronically to match the order of experiments in (*B*). Bar graphs represent quantitation of bands from at least 3 independent experiments.

Figure 1.2 Quantification of EGFR expression in CHO stable cell lines

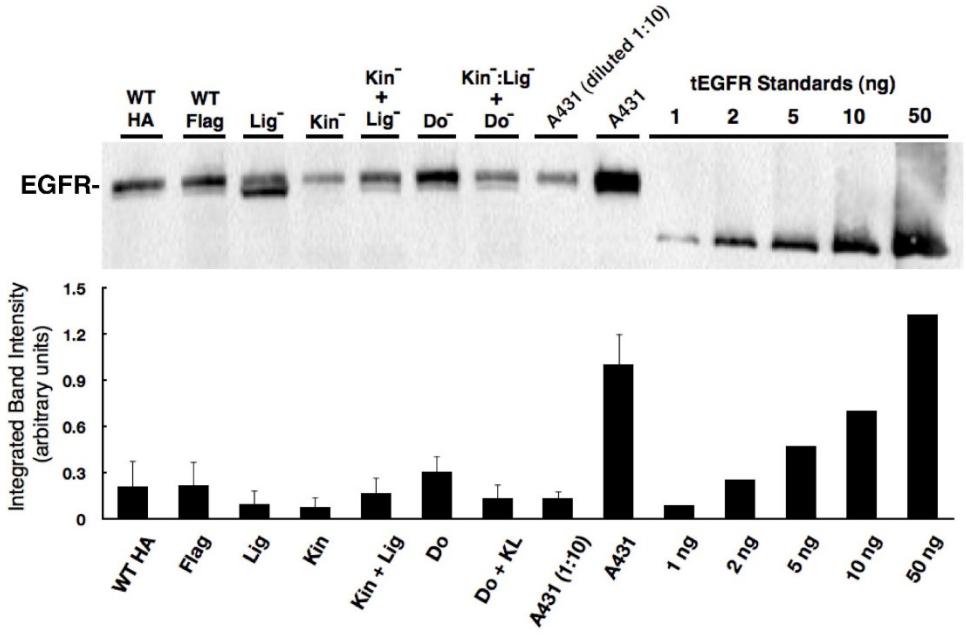

Figure 1.2 Anti-EGFR Western blots of lysates from known numbers of the EGFR-transfected cells used in cell-based assays, as well as A431 cells. Cell lines are labeled as in Figure 1.1. Known amounts of purified, truncated EGFR were loaded as standards (right 5 lanes).

Table 1.1 Identities of Plasmids and Mutations for ErbB-expressing stable cell lines

EGFR-transfected Cell Line	Plasmid 1 Tag – Amino-acid Substitution(s)	Plasmid 2 Tag – Amino-acid Substitution(s)
HA-WT	HA	-
Flag-WT	Flag	-
Flag-Lig	Flag-D355A	-
HA-Kin	HA-D813N	-
Flag-Lig/HA-Kin	Flag-D355A	HA-D813N
HA-Dim	HA-Y251A+R285S	-
Flag-Dim+Lig	Flag-Y251A+R285S+D355A	-
HA-Dim+Kin	HA-Y251A+R285S+D813N	-
Flag-Dim+Lig/HA-Kin	Flag-Y251A+R285S+D355A	HA-D813N
Flag-Lig/HA-Dim+Kin	Flag-D355A	HA-Y251A+R285S+D813N
HA-Do	HA-V924R	-
Flag-Lig+Kin/HA-Do	Flag-D355A+D813N	HA-V924R
ErbB4-transfected Cell Line		
HA-WT	HA	-
Flag-WT	Flag	-
HA-Lig	HA-D351R	-
Flag-Kin	Flag-D818N	-
Ha-Lig/Flag-Kin	HA-D351R	Flag-D818N
HA-Dim	HA-F248A+R281S	-
HA-Dim+Lig	HA-F248A+R281S+D351R	-
Flag-Dim+Kin	Flag-F248A+R281S+D818N	-
HA-Dim+Lig /Flag-Kin	HA-F248A+R281S+D351R	Flag-D818N
Flag-Dim+Kin/HA-Lig	Flag-F248A+R281S+D818N	HA-D351R
Flag-Do	Flag-V929R	-
HA-Lig+Kin/Flag-Do	HA-D351R+D818N	Flag-V929R

Table 1.2 Average number of EGF receptors in ErbB1-expressing cell lines

Cell Line	EGF Receptors per cell
WT HA	130,000
WT Flag	128,000
Lig-	60,000
Kin-	53,000
Kin- + Lig-	87,000
Do-	179,000
Do- + K-:L-	72,000
A431	1,900,000

Chapter 2: How IGF-1 activates its receptor

Note to reader: this chapter contains excerpts from (Kavran, et al., 2014). It has been edited for clarity where appropriate.

Acknowledgements

This work was performed in collaboration with Jennifer Kavran, Jackie McCabe, MK Connacher, and Sarvenaz Sarabipour at Johns Hopkins University. Thanks for their work in preparing the cell lines and reagents necessary for these experiments, and their advice in troubleshooting technical issues. Jennifer Kavran and Dan Leahy performed the structural analysis of the IGF1R extracellular domain. Molecular dynamics simulations were performed by Yibing Shan at the DE Shaw Research Institute.

Abstract

The type I insulin-like growth factor receptor (IGF1R) is involved in growth and survival of normal and neoplastic cells. A ligand-dependent conformational change is thought to regulate IGF1R activity, but the nature of this change is unclear. We point out an underappreciated dimer in the crystal structure of the related Insulin Receptor (IR) with Insulin bound that allows direct comparison with unliganded IR and suggests a mechanism by which ligand regulates IR/IGF1R activity. We test this mechanism in a series of biochemical and biophysical assays and find the IGF1R ectodomain maintains an autoinhibited state in which the TMs are held apart. Ligand binding releases this constraint, allowing TM association and unleashing an intrinsic propensity of the

intracellular regions to autophosphorylate. Enzymatic studies of full-length and kinase-containing fragments show phosphorylated IGF1R is fully active independent of ligand and the extracellular-TM regions. The key step triggered by ligand binding is thus autophosphorylation.

Introduction

The insulin and type-1 insulin-like growth factor receptors (IR and IGF1R) are homologous receptor tyrosine kinases (RTKs) that regulate cell metabolism, growth, and differentiation in a variety of mammalian tissues (De Meyts, 2004) (Siddle, 2011) (Siddle, 2012). Each is essential for normal development (Liu, et al., 1993) (Accili, et al.,, 1996), and abnormal IR or IGF1R signaling is associated with many disorders, notably diabetes and cancer (De Meyts & Whittaker, 2002) (Pollak, 2012). Although IGF1R is mainly associated with cell growth and differentiation and IR with regulation of glucose and lipid metabolism (Siddle, 2012), IGF1R and IR share 58% sequence identity and appear to signal via largely conserved molecular mechanisms (Siddle, 2011) (Ward, et al., 2013).

IR and IGF1R are disulfide-linked homodimers of single-pass integral membrane protein subunits. Each subunit undergoes a furin-like cleavage into α and β chains that remain disulfide-linked and are composed of six extracellular domains (L1, CR, L2, Fn1, Fn2, and Fn3) followed by a transmembrane (TM) region, a ~30 amino acid juxtamembrane region, a tyrosine kinase domain, and a C-terminal tail (Ullrich, et al.,, 1985) (De Meyts & Whittaker, 2002) (Figure 2.1A,B). An ~110 a.a. nonglobular

insertion in Fn2, termed the insert domain (ID), contains the cleavage site and three cysteines of which one or more form reciprocal inter-subunit disulfide bonds. An additional inter-subunit disulfide is formed between cysteines in Fn1 (Cheatham, et al., 1993) (Schaffer & Ljungqvist, 1992) (Sparrow, et al., 1997).

Ligand binding to IR and IGF1R extracellular regions (ECDs) stimulates receptor kinase activity, leading to phosphorylation of multiple substrates and initiation of specific signaling cascades (Siddle, 2012). IR family members are unique among RTKs in forming constitutive dimers (of αβ subunits). Dimerization per se thus cannot be the activating signal, and activation is thought to involve a ligand-dependent conformational change (Frattali, et al., 1992) (Lemmon & Schlessinger, 2010). Part of the function of the ECD appears to be maintaining an inactive state in the absence of ligand as tryptic removal of the IR ECD results in constitutive activity (Tamura, et al., 1983) (Shoelson, et al., 1988).

Two ligand-binding sites are present in each αβ dimer. Each site is composed of two distinct partial sites known as 'Site 1', which is composed of residues on L1 from one subunit and residues on the αCT′ helix of the other subunit (a prime is used to indicate the opposite subunit), and 'Site 2', which is composed of residues on Fn1′ and Fn2′ (Williams, et al., 1995) (Mynarcik, et al., 1996) (Whittaker, et al., 2001) (Whittaker, L, et al., 2008) (Smith, et al., 2010). A classic feature of ligand binding to IR and IGF1R is negative cooperativity (De Meyts, 2004), which implies communication between the two sites such that ligand binding to one site generates an asymmetric state of the

receptor in which the affinity of the second site for ligand is weakened. The nature of this asymmetric state is not known, but hydrogen–deuterium exchange experiments with IGF1R identified regions that are likely foci of this asymmetry (Houde & Demarest, 2011).

To address the gaps in our understanding of the molecular mechanisms underlying IR family activation, we performed a series of biochemical and biophysical assays and show that the IGF1R ECD indeed autoinhibits activity by holding the TMs apart in the absence of ligand. Ligand binding releases this autoinhibition and allows the TMs to come together in an autophosphorylation-competent state. The key step regulated by ligand binding is thus autophosphorylation and not kinase activity per se, and the role of the IR/IGF1R ECD is to inhibit activity in the absence of ligand rather than promote activity in the presence of ligand.

Results

Release of IGF1R autoinhibition by ligand brings the TMs together

Loss of either the L1 domain or the ECD eliminates the inter-subunit interaction between L1:Fn2′–3′ that fixes the separation of the TM regions (Kavran, et al., 2014). To examine if TM separation is altered in active receptors, we replaced the intracellular domain (ICD) of IGF1R with fluorescent donor or acceptor proteins (IGF1R ECD-TM-fp) and determined the FRET efficiency between co-transfected donor–acceptor pairs in the presence and absence of ligand (Figure 2.3). We used spectrally resolved Förster resonance energy transfer (FRET) (Raicu, et al., 2008) to calculate the FRET efficiency

at the pixel level in transfected CHO cells, which ensures only proteins expressed at the cell membrane are included in the analysis. FRET efficiency increased twofold in the presence of ligand (Figure 2.3A). Assuming comparable if not random orientations of the fluorescent proteins in both states, these data indicate the C-termini of the TMs move closer together in the presence of ligand. A similar increase in FRET efficiency was observed in vesicles derived from CHO cells expressing IGF1R ECD-TM-fp in the presence and absence of ligand (Figure 2.4). We also measured the FRET efficiency for IGF1R lacking the L1 domain (IGF1R ECDΔL1-TM-fp) and found that its FRET efficiency is similar to that of IGF1R ECD-TM-fp with bound ligand suggesting that the ligand bound state of IGF1R is similar to that of the receptor when the L1:Fn2′–3′ interface is disrupted (Fig. 2.4).

If the IGF1R ECD inhibits IGF1R activity by enforcing TM separation, introduction of flexible linkers between the ECD and TM regions should release this inhibition, and insertion of progressively longer linkers composed of glycine–serine containing repeats between 4 and 20 residues long indeed led to increasing levels of basal receptor activity (Figure 2.3B).

Isolated IGF1R TMs dimerize

The ligand-dependent decrease in distance between IGF1R TMs observed in FRET assays of IGF1R ECD-TM-fp led to the question of whether IGF1R TMs physically associate in the active state. Analysis of IR family TM sequences failed to identify any motifs known to mediate TM interactions, such as GXXXG (Russ &

Engelman, 2000), but did identify an absolutely conserved proline (P911 in human IGF1R) (Figure 2.5A). To investigate the role of P911 in receptor activation, we performed cell based activity assays with IGF1R-fl bearing either a single P911L substitution or with additional substitutions to residues surrounding P911. These IGF1R variants became phosphorylated in a ligand-dependent manner suggesting P911 does not play a key role in mediating receptor activity, an outcome consistent with the results of earlier studies involving more dramatic manipulations of IR TM residues and suggesting lax constraints on TM sequence (Fratalli, et al., 1991) (Yamada, et al., 1992) (Cheatham, et al., 1993) (Figure 2.5).

Experimental evidence that IGF1R TMs have an intrinsic propensity to dimerize in bilayers was obtained from quantitative imaging FRET (QI-FRET) experiments (Li, et al., 2008). Isolated IGF1R TMs were fused to C-terminal donor or acceptor fluorescent proteins (IGF1R TM-fp) and transiently transfected into CHO cells (Fig. 2.5). Vesicles containing variable amounts of expressed proteins were generated and FRET efficiency analyzed (Chen, et al., 2010a) (Del Piccolo, et al., 2012). FRET efficiency increased as a function of fluorescent protein concentration and exceeded the theoretical levels of FRET expected to arise from random proximity (King, et al., 2014), demonstrating an intrinsic propensity of IGF1R TMs to associate (Figure 2.5C).

An intrinsic propensity of IGF1R TM and ICD regions to dimerize was also demonstrated by cysteine substitutions in constitutively active ECD-truncated forms of IGF1R (IGF1R TM-icd) (Figure 2.5D). The side chains of the extracellular membrane-

proximal residue H905 approach within 6 Å of one another in the MD dimer (Figure 2.5B), and H905 or T898 were individually substituted with cysteine in IGF1R TM-icd variants. Western blots of reduced and non-reduced lysates from HEK293 cells expressing these proteins show that the majority of the H905C variant forms a disulfide-linked dimer (Figure 2.5D). Lower amounts of dimerization were observed for the T898 variant in which the cysteines are farther away from the TM region (Figure 2.5D), and no disulfide crosslinking was observed for an equivalently truncated IGF1R without a cysteine substitution. These results demonstrate that, in the absence of the ECD, the IGF1R TM-icds come together in a manner consistent with the MD TM dimer.

IGF1R TMs dimerize in the active, full-length receptor

We next investigated whether juxtamembrane cysteines formed disulfide crosslinks when introduced into IGF1R-fl (Figure 2.6A). We could not directly analyze intra-dimer disulfide bond formation by introduced cysteines by analyzing migration on reducing and non-reducing SDS-PAGE owing to the native disulfide bonds linking α and β chains. To circumvent this issue, we substituted the cysteine residues that mediate the αβ disulfide with serine. These substitutions inhibited proper proteolytic processing of the receptor, however, obscuring differentiation of the new disulfide bond from native disulfide bonds. To our surprise, however, Western blots monitoring the phosphorylation of the IGF1R variants with the single substitutions of either T898C or H905C revealed high levels of phosphorylation in the absence of ligand (Figure 2.6A). An IGF1R-fl variant with a cysteine substitution immediately following the Fn3 domain and further

away from the TM (Q895C) displayed only a modest increase in basal phosphorylation compared to wild-type (Figure 2.6A), perhaps owing to steric interference from Fn3 domains.

An intra-dimer disulfide between cysteines at position 905 would force TM association. When the H905C substitution was introduced into IGF1R ECD-TM-fp, the FRET efficiency of this variant in the absence of ligand matched that of native IGF1R ECD-TM-fp in the presence of ligand (Figure 2.6B). This result shows that the H905C substitution indeed leads to decreased TM separation, presumably owing to crosslinked juxtamembrane regions, and that this conformation is indistinguishable from that observed for liganded IGF1R ECD-TM-fp.

Discussion

We describe a molecular mechanism for IR/IGF1R activation in which ECD-enforced separation of TMs maintains the receptor in an inhibited state. Ligand binding relieves this inhibition by disrupting the L1:Fn2′–3′ interaction that stabilizes TM separation, freeing the TMs to associate and autophosphorylation of the kinase domains to proceed (Figure 2.7). This model is based on a previously underappreciated dimer in the crystal structure of an Insulin bound IR ECD fragment, which provides a basis for comparing liganded and unliganded structures of the IR ECD.

To validate this model, we present FRET and mutagenesis studies that demonstrate (i) a decrease in IGF1R TM separation when ligand binds, (ii) an intrinsic propensity of the IGF1R TM and TM-icd to dimerize, (iii) that the kinase is active in this

associated state, consistent with the increased activity of the IGF1R ICD when fused to a dimeric partner (Baer, et al.,, 2001) (iv) that the role of the ECD is primarily to inhibit this intrinsic kinase activity in the absence of ligand, rather than promote a specific active state, (v) that IGF1R TMs associate in an active form of the full-length receptor, and (vi) that IGF1R samples the active state even in the absence of ligand. Enzymatic studies of full-length IGF1R and IGF1R fragments further demonstrate no role for allostery in maintaining IGF1R activity once it is phosphorylated, indicating that the key step regulated by ligand binding is autophosphorylation. Although ligand binding has no effect on the intrinsic activity of phosphorylated IGF1R, the short half-life of IGF1R phosphorylation when phosphatases are present suggests the continued presence of ligand may be needed to maintain IGF1R activity (Kleiman, 2011). This efficiency of cellular phosphatases may also explain why transient sampling of the active state by IGF1R does not lead to constitutive activity.

Previous models for IR activation have posited only modest changes in receptor conformation when ligand binds and that 'twist' rather than lateral movement of the Fn2–3 domains is the activating signal or that the TM regions move from associated to apart during IR activation (Ward, et al., 2013) (Lee, et al., 2014). We show here that ligand binding to IGF1R leads to TM association. Thus the Fn2–3 domains must undergo a large movement upon ligand binding to accommodate the new position of the TMs. To model this movement, we appended the Fn2–3 tandems from the unliganded IR ECD structure to the structure of the IR ECD fragment bound to Insulin. The Fn2–3 tandems were then manually repositioned using only the constraints that the ligand bound position of these

'legs' must be compatible with the TM dimer observed in MD simulations and that the residues on Fn2 that compose Site 2 contact ligand. Assuming the connection between Fn1 and Fn2 to be flexible (it buries ~500 $Å^2$ of surface area) and the Fn2–3 tandem to be rigid, we find it possible to place the Fn2–3 tandems so that Site 2 residues appose ligand and that the ECD C-termini are compatible with TM dimerization (Figure 2.7B–D).

We have modeled IR/IGF1R with two bound ligands (Figure 2.7D) but receptors with a single ligand bound may represent an important active state. Negative cooperativity implies that ligand binding at one site influences assembly of the second site. The most likely conduit of information between sites is through the αCTs, which are connected by an inter-subunit disulfide bond 8 residues from their N-termini. The αCTs are 30 Å farther apart in the liganded IR structure than in the unliganded IR structure (Smith, et al., 2010) (Menting, et al., 2013). This increased separation is only possible because the inter-subunit disulfides that link the αCTs were deleted in the crystallized fragment of IR. In an intact receptor, the altered position of αCT following binding of one ligand would restrict the reach of the opposite αCT, likely hindering assembly of the second binding site and contributing to negative cooperativity.

The intrinsic propensity of the TMs to associate may also contribute to negative cooperativity. Disruption of the L1:Fn2′–3′ interaction by ligand binding removes a restraint on the relative position of the TMs that served as a barrier to TM association (Figure 2.2). Decreasing this barrier may shift the energetic balance between maintenance

of the L1′:Fn2–3 interaction at the unliganded site and the intrinsic propensity of the TMs to associate and couple TM association to rearrangement of elements of the unliganded binding site. This mechanism may underlie the restoration of negative cooperativity of soluble IR ECDs when their C-termini are artificially tethered (Hoyne, 2000).

The results discussed so far implicate ECD-enforced TM separation as a key feature maintaining IGF1R and IR inactive states. The question then arises of how TM separation maintains the kinases in an inactive state. The simplest explanation is that spatial separation is sufficient to preclude one kinase from phosphorylating the other. The N-termini of subunits of an IGF1R kinase dimer captured in an apparent *trans* phosphorylation state are ∼50 Å apart (Wu et al., 2008), however, and the 27 residues separating each kinase domain from its TM could easily span the distance needed to reach the ∼120 Å separation imposed by the ECD. The IGF1R intracellular juxtamembrane regions must thus adopt some structure in the inactive state to preclude autophosphorylation, but secondary structure prediction algorithms only identify a short 7 amino-acid β strand in this region. Outside of three positively charged residues immediately following the TM, no conserved regions of positive charge comparable to the region in EGFR thought to mediate interactions with the membrane are present (Jura, 2009). Conversely, the fourfold enhancement of kinase activity when the juxtamembrane region is present implies some structure in this region in the active state. Attempts to identify regions of the IGF1R kinase important for maintaining the inactive state by either mutagenesis or inspection of kinase crystal lattices for a repeated interaction proved unsuccessful, however. No IGF1R kinase surface mutations led to higher basal

activity, and no repeated interactions or regions of positive charge are apparent in IGF1R kinase crystals that could mediate self interactions or interactions with the plasma membrane as has been proposed for EGFR (Arkhipov, et al., 2013).

In contrast, the absence of allosteric enhancement of the activity of phosphorylated IGF1R implies the absence of a stable interaction between kinase domains in the active state. Consistent with this conclusion, surface mutagenesis of the IGF1R kinase demonstrates the absence of an EGFR-like asymmetric kinase dimer. Absence of allostery in the active state may be a general feature of RTKs whose activity is enhanced by multiple activation loop phosphorylations, including FGFR, Met, VEGFR, Alk, MUSK, Kit, and their homologs (Lemmon & Schlessinger, 2010). Transient intermediate states may direct the order of tyrosines phosphorylated, as observed for FGFR (Lew, et al., 2009), but once fully phosphorylated we suspect the activity of these kinases will also prove independent of allosteric stimulation. This behavior contrasts with that of EGFR, which relies on allostery via a kinase asymmetric dimer for activation rather than phosphorylation of the activation loop (Zhang, et al., 2006).

Although IGF1R ICDs do not appear to form a stable interaction in the active state, TM dimerization does appear to occur upon ligand binding. This observation is consistent with previous studies demonstrating a coupling between ligand binding and association of IR ECD C-termini as well as results with chimeric receptors. When the IR ECD is expressed in soluble form it binds with nearly 1000-fold lower affinity than full-

length IR, but when the C-termini of the ECD are fused to either a leucine zipper (Hoyne, 2000) or an immunoglobulin Fc region (Bass, et al., 1996), high-affinity, native-like ligand binding is restored (Schaffer, 1994). TM dimerization is thus not only consistent with high-affinity ligand binding but promotes it. Furthermore, a chimeric receptor with an IR ECD and an EGFR TM and ICD can be activated by Insulin (Reidel, et al., 1986). As EGFR activation involves TM dimerization (Endres, et al., 2013), the Insulin-bound IR ECD is also compatible with TM dimerization.

We present here a new molecular model for regulation of IGF1R and IR activity. The key feature of this model is maintenance of an inactive state by ECD-enforced separation of the TMs in the absence of ligand. Ligand binding releases this constraint, resulting in TM association and unleashing of the intrinsic propensity of the kinase regions to autophosphorylate and activate. This model is consistent with recent crystal structures of the IR ECD and suggests that some structure in the intracellular region precludes autophosphorylation in the unliganded state of the receptor. Conversely, enzymatic studies show that once phosphorylated and active, no structure outside of the kinase and juxtamembrane regions is needed to stimulate full kinase activity. This model provides a simple molecular context for understanding several features of IR/IGF1R activation and suggests directions for future study. It also suggests that chimeric proteins with IR or IGF1R ECDs may prove valuable for assessing the role of TM separation in other signaling systems or as ligand-dependent activity switches when fused, for example, to split enzymes.

Materials and Methods

Expression and purification of fluorescent proteins

Plasmids encoding N-terminally hexa-histidine tagged EYFP, mCherry, or mTurquoise were transformed into *Escherichia coli* BL21(DE3) cells. Cultures were grown in Luria Broth at 37°C to OD_{600} ~0.6, and the temperature dropped to 18°C for 30 min. IPTG was added to a final concentration of 1 mM, and the culture was grown overnight (~16 hr). Cells were harvested by centrifugation and lysed using a French pressure cell. An IMAC column was loaded with clarified lysate, washed with 20 mM imidazole, and eluted with 250 mM imidazole. Protein-containing fractions were pooled, dialyzed, concentrated, and flash frozen. To minimize photobleaching, all expression and purification steps were performed in the dark. The purity of the fluorescent proteins was >90% after the nickel column as judged by Coommassie Brilliant Blue stained SDS-PAGE.

Cell-based IGF1R activity assays

IGF1R cell-based assays were based on established procedures (Liu, et al., 2012). HEK293 cells (ATCC) were maintained in adherent culture in DMEM:F12 supplemented with 5% FBS. HEK293 cells were chosen due to low background endogenous IGF1R as judged by Western blot and equal transfection efficiency of IGF1R wild-type and kinase-inactive (D1205A/N) when compared with transient transfection of *igf1r* (−/−) mouse embryonic fibroblasts (a generous gift from R Baserga). HEK293 cells were plated in a six-well plate at 1×10^6 cells/well and transiently transfected with IGF1R expression plasmids using polyethylenimine (PEI, linear MW 25,000; Polysciences, Inc.,

Warrington, Pennsylvania) at an optimized ratio of 1 μg DNA: 3 μg PEI. Variant IGF1R genes were subcloned into pSSX-F, a version of pSGHV0 modified to eliminate the growth hormone tag and add a C-terminal Flag tag (Leahy, et al., 2000). After 18 hr, cells were washed three times with 2 ml Ham's F12 supplemented with 1 mg/ml BSA and incubated in this medium for 3 hr at 37°C to serum starve. In designated wells, 20 nM IGF1 was added and incubated for 30 min at 37°C.

For cross-linking assays and assays using truncated IGF1R variants, the wells were washed with ice-cold phosphate buffered saline and then lysed for 30 min at 4°C in 250 μl of RIPA buffer (50 mM Tris pH 8, 150 mM NaCl, 1% NP-40, 0.5% sodium deoxycholate, and 0.1% SDS) supplemented with 1 mM activated Na_3VO_4, 1 mM PMSF, Benzonase nuclease (Sigma), and 10 mM iodoacetamide to prevent further disulphide-bond formation during lysis (Cao, et al., 1992). Lysates were clarified and samples were separated by either denaturing reducing or non-reducing SDS-PAGE electrophoresis. Western blot analysis was performed using anti-IGF1Rβ (Santa Cruz Biotechnologies, Dallas, Texas) Western blots were developed using ECL2 (Thermo Scientific) and scanned using a Typhoon Imager. Bands corresponding to phosphorylated IGF1R from the 4G10 Western blot were quantified using ImageJ and normalized to receptor expression from quantified bands of the IGF1R-β Western blot for each experiment.

For autophosphorylation analysis, the wells were washed with ice-cold phosphate buffered saline and lysed in supplemented RIPA buffer lacking iodoacetamide. The cell suspension was clarified, and total protein concentration determined using the BCA protein assay (Thermo Scientific-Pierce) to normalize cell lysates. For assays with

truncated IGF1R proteins, Western blot analysis was performed on cell lysates using anti-IGF1Rβ or anti-IGF1R phosphotyrosine 1135 (pY1135) (Cell Signaling Technology, Danvers, Massachusetts) antibodies. For assays with IGF1R-fl proteins with kinase clusters, single cysteine substitutions, or TM mutations immunoprecipitation was performed. Anti-Flag-M2 (Sigma) was added at 0.5 μg/ml to lysate followed by the addition of 20 μl Protein G Sepharose 4 Fast Flow (GE Healthcare). Lysates were then incubated overnight at 4°C. Beads were then washed three times with 1 ml of RIPA buffer supplemented with 1 mM activated Na_3VO_4. Beads were eluted by the addition of 20 μl of 5× LDS loading buffer containing 10% fresh β-mercaptoethanol. Equal amounts of eluted proteins were analyzed as described for the cross-linking analysis but using both anti-pY and anti-IGF1Rβ antibodies.

Confocal microscopy and quantitative imaging FRET

CHO cells were cultured in DMEM-F12 supplemented with 5% FBS and 1 mM *L*-glutamine. Cells were seeded in 35-mm dishes at a density of 4×10^4 cells per well and grown for 24 hr at 37°C in 5% CO_2, then transiently co-transfected with plasmids encoding IGF1R TM-EYFP (3 μg) and IGF1R TM-mCherry (6 μg) using the Fugene HD transfection reagent at a mass ratio of 3:1 (Fugene:DNA) according to the manufacturer's protocol.

After 24 hr, cells were washed twice with 1 ml of 30% PBS, one minute per wash. 1 ml of chloride salt vesiculation buffer (Del Piccolo, et al., 2012) was added to each well, and the wells were incubated at 37°C, 5% CO_2. Vesiculation buffer is composed of 200 mM NaCl, 5 mM KCl, 0.5 mM $MgCl_2$, 0.75 mM $CaCl_2$, and 100 mM bicine, pH 8.5.

Vesiculation reached completion after about 12 hr, and the entire well supernatant was transferred to 4-well chambered slides (Thermo Scientific, Nunc Lab-Tek II). The wells were allowed to equilibrate to room temperature before imaging.

Vesicle images were acquired using a Nikon C1 laser scanning confocal microscope equipped with a 60× water immersion objective. Three scans were taken for each vesicle: (i) a 'donor' scan (λ_{exc} = 488 nm, λ_{em} = 500–530 nm), (ii) an 'acceptor' scan (λ_{exc} = 543 nm, λ_{em} = 650 nm longpass), and (iii) a 'FRET' scan (λ_{exc} = 488 nm, λ_{em} = 565–615 nm). The donor and FRET scans used a 488 nm argon ion laser excitation source, while the acceptor scan used a 543 nm He-Ne laser. The image resolution was 512 × 512 pixels, with a pixel dwell time of 1.68 μs. The gains were set to 7. All images were processed using a Matlab program developed in the Hristova laboratory. The program finds the boundary of each vesicle, verifies that the vesicle is present in all three scans, and fits the intensity profile across the membrane to a Gaussian function. The baseline is fitted with an error function. Details for the calculations of FRET efficiency are provided in the study by (Chen, et al., 2010a) (Chen, et al., 2010b) We calculated the intrinsic FRET efficiency as:

$$\text{Intrinsic FRET} = (E_{app} - E_{proximity})/X_a$$

where E_{app} is the apparent FRET efficiency observed in each vesicle, $E_{proximity}$ is contribution of FRET from nonspecific interactions (King, et al., 2014), and X_a is a correction factor which accounts for varying ratios of donor and acceptor molecules within each vesicle.

To determine fluorescent protein concentration in the vesicles, vesicle fluorescence intensities were normalized to standard solutions of mCherry and EYFP purified from *E. coli* BL21 cells using the formula (Chen, et al., 2010a) (Chen, et al., 2010b):

$$E = 1 - I_mDI_mD + I_mD_{,corr}$$

where *ImD* is the emission intensity of the donor per unit area of the membrane in the presence of RET, and *ImD*,*corr* is the donor emission intensity in the absence of RET. Bleed-through coefficients were calculated from confocal images of standard solutions of purified EYFP and mCherry. Using absorption and emission spectra of purified proteins, we calculated the Förster radius for the EYFP-mCherry donor–acceptor pair to be 53.1 Å.

Two photon FRET microscopy on living cells

We employed two donor–acceptor FRET pairs for this study: mTurquoise-YFP and YFP-mCherry. We calculated the Förster radius for each pair to be 54.5 Å (mTurquoise-EYFP) and 53.1 Å (EYFP-mCherry), making them suitable for investigating conformational changes on the order of 30–90 Å. CHO cells were cultured in 35-mm collagen-coated glass bottomed dishes (MatTek Corporation, Ashland, Massachusetts) using phenol red-free DMEM-F12 supplemented with 5% FBS and 1 mM *L*-glutamine. Plasmids encoding the IGF1R extracellular and transmembrane regions fused after GGSGGS to mTurquoise (FRET donor) or EYFP (FRET acceptor) were co-transfected using Fugene HD (Promega, Madison, Wisconsin) at a mass ratio of 3:1

(Fugene:DNA), according to the manufacturer's protocol. Transfection proceeded for 24 hr at 37°C, 5% CO_2.

We used the OptiMiS TruLine Spectral Scanning System (Aurora Spectral Technologies, Milwaukee, Wisconsin) for two-photon microscopy. A solid-state continuous wave laser pumped a mode-locked Ti:Sapphire laser (MaiTai DeepSee, Newport Corporation, Irvine, California) that generated near infrared pulses in the wavelength range of 800–960 nm (λ_{exc} for mTurquoise = 800 nm; λ_{exc} for eYFP = 960 nm). The beam was focused using a 63× objective (Nikon, Japan). Fluorescence emission from the sample chamber was projected through a transmission grating onto a cooled electron-multiplying charge-coupled device. The full spectral scans of all pixels in the viewing field (300 × 440 pixels) were completed in about 10 s.

Image acquisition and processing are based on the method described by Raicu et al. (2008). Prior to imaging, CHO cells were washed three times in 1× PBS to remove all traces of FBS, then serum starved in phenol red-free DMEM-F12 without FBS. After 5 hr of starvation, the media were changed a final time and the cells were imaged directly in the two-photon microscope. Individual donor and acceptor fluorescence spectra were collected from cells expressing either the donor- or acceptor-fused IGF1R alone. A single 'FRET' scan ($\lambda_{exc,\ two\ photon}$ = 800 nm) was acquired for each cell that coexpressed both EYFP and mTurquoise-fusion proteins. The full spectral emission profile was collected from 450–600 nm (1 nm resolution), and the FRET efficiency per pixel (*EDapp*) was calculated using a Matlab program, according to the equations described (Raicu, et al., 2008):

$$E^{Dq}_{app} \equiv F_{D(RET)}F_{D(\lambda ex)=} = 11+Q^{A}Q^{D}k^{D}{}_{A}k_{AD}w_{D}w_{A}$$

where $F_{D(RET)}$ and $F_{D(\lambda ex)}$ equal the fluorescence emission of the donor in the presence and absence of resonance energy transfer, respectively. Q^{A} and Q^{D} are the quantum yields of the donor an acceptor fluorophore, and k^{DA} and k^{AD} are the maximum emission intensities of the donor in the presence of the acceptor, and the acceptor in the presence of the donor, respectively. The integrals of the individual emission spectra for the donor and acceptor are given by w^{D} and w^{A}. Representative pixels in each cell membrane were examined by eye to ensure a good fit to the FRET model. We calculated the Förster radius for the mTurquoise-EYFP donor–acceptor pair to be 54.5 Å using measured absorption and emission spectra from purified proteins (King, et al., 2014).

Figure 2.1. The extracellular domain of IGF1R autoinhibits IGF1R activity.

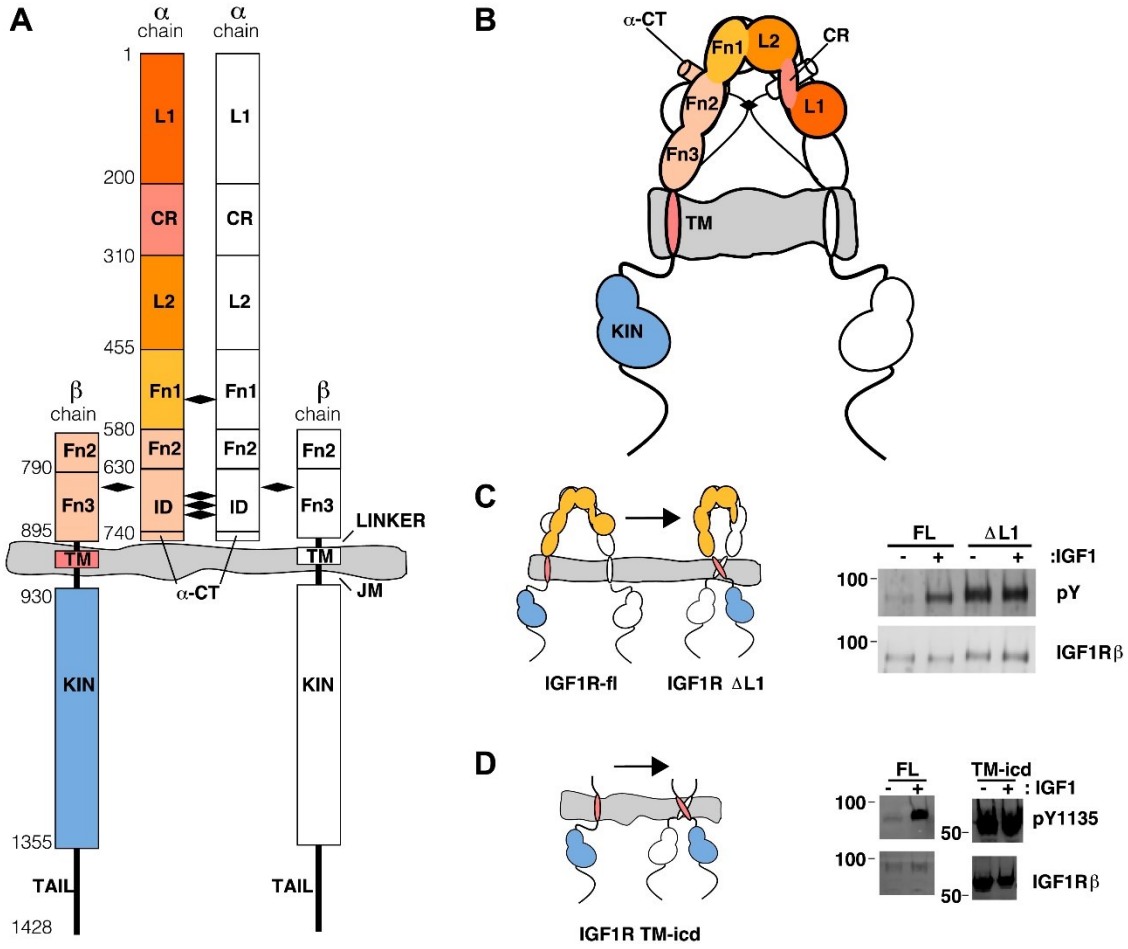

Figure 2.1. (**A**, **B**) Schematic and cartoon representations of IGF1R. Numbering refers to human IGF1R excluding the signal sequence. Disulfide bonds are indicated by black diamonds. One αβ subunit is shown in outline and the other in color. (**C**) Cartoon of IGF1R full-length (IGF1R-fl) or an IGF1R fragment lacking the L1 domain (IGF1R ΔL1) (left). HEK293 cells expressing either IGF1R-fl (FL) or IGF1R ΔL1 (ΔL1) were incubated with or without IGF1. IGF1R proteins were immunoprecipitated from normalized cell lysates and levels of autophosphorylation or IGF1R expression detected by Western blot with anti-phosphotyrosine (pY) or anti-IGF1Rβ antibodies (right).

Molecular weight standards indicated to the left of each panel (**D**). Diagram of IGF1R variant lacking the ECD (IGF1R TM-icd) (left). Western blots probed with anti-pY1135, which recognizes a phosphotyrosine on the activation loop of the IGF1R kinase domain, and anti-IGF1Rβ of normalized lysates from cells expressing IGF1R-fl (FL) or IGF1R TM-icd (TM-icd), in the presence and absence of IGF1 (right). All panels are from the same blot. See also supplemental figures.

Figure 2.2. Conserved IR ECD dimer interaction.

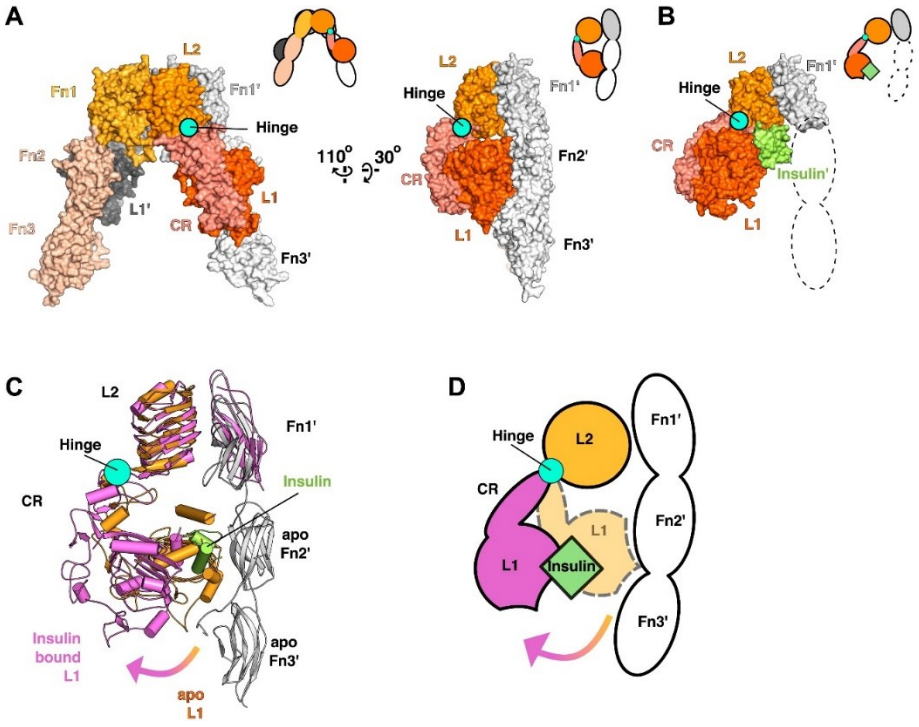

Figure 2.2. (**A**) Surface representation of the unliganded IR ECD (PDB 3LOH; (Smith, et al., 2010)) oriented to show the L1:Fn2'-3' interface. The hinge between CR and L2 is indicated by a cyan circle. Cartoons of domains shown are to the upper right of each structure. (**B**) Surface representation of ligand-bound IR ECD fragment (PDB 3W14; (Menting, et al., 2013)) in the same orientation as in **A**. The missing Fn2-3 domains are indicated by dashed lines. (**C**) Superposition of the ligand-bound IR structure (purple ribbon) onto the unliganded structure (orange and white ribbon) using the L2-Fn1 domain pairs. Insulin is displayed in light green. An arrow shows the direction of the relative movement of unsuperposed L1-CR domains about a hinge (cyan circle) between the CR and L2 domains. Complementary halves of each receptor subunit were omitted for clarity. (**D**) A cartoon showing the movement of the L1-CR domain tandems.

Figure 2.3. The IGF1R ECD maintains TM separation

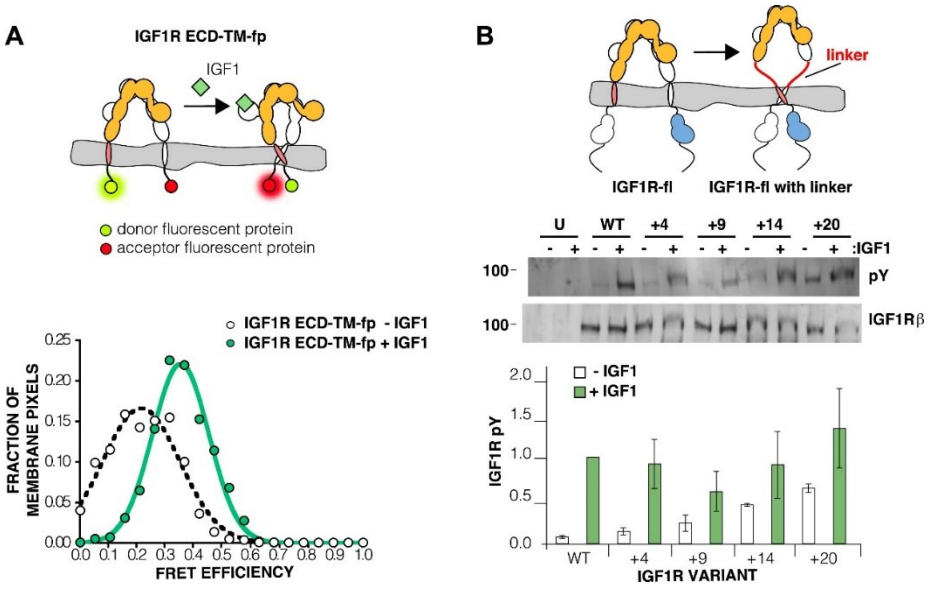

Figure 2.3. (**A**) Cartoon of the IGF1R ECD-TM-fp variant utilized in the live cell FRET assay (top). Frequency distribution of FRET efficiency values per membrane pixel of IGF1R ECD-TM-fp in the presence (green) or absence (white) of IGF1 (bottom). Data were fit to a normal distribution with peak values of 0.34 ± 0.09 and 0.21 ± 0.13 in the presence and absence of IGF1, respectively. (**B**) Cartoon of the IGF1R-fl and IGF1R variants with flexible linkers (top). Representative western blots probed with either anti-pY and anti-IGF1Rβ antibodies of immunopreciptated, normalized cell lysates of untransfected cells (U) or cells transfected with IGF1R-fl (WT) or IGF1R variants with an additional 4 (+4), 9 (+9), 14 (+14), or 20 (+20) glycine and serine residues per αβ chain (middle). Bar graph of average IGF1R phosphorylation normalized to total receptor concentration (±s.e.m.) from at least three separate experiments, except for +14 which was from 2. Results from cells incubated in the absence of IGF1 are shown in white and in the presence of IGF1 shown in green (bottom). See also supplemental figures

Figure 2.4. Intrinsic FRET efficiency in vesicles, corrected for proximity FRET and varying donor-to-acceptor ratios.

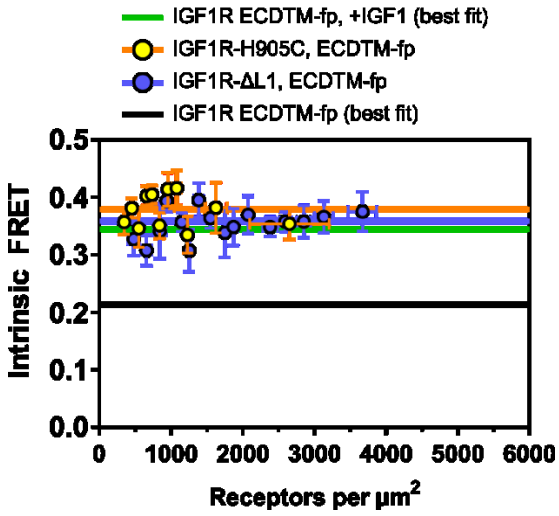

Figure 2.4. Intrinsic FRET efficiencies between isolated IGF1R TM-fp (pink circles), IGF1R ECD-TM-fp with IGF1 (green circles) or without IGF1 (white circles), IGF1R ECD-ΔL1-TM-fp (blue circles), and IGF1R ECD-TM-fp H905C (yellow circles), plotted as a function of the total receptor, IGF1R-YFP and IGF1R-mCherry, concentration. Each data point represents the binned FRET efficiency measured from at least eight vesicles (±s.e.m. in x and y). Intrinsic FRET is the observed FRET corrected for differences in expression of donor and acceptor proteins and corrected for FRET resulting in random proximity. The remaining data were fit to a horizontal line with y intercept of 0.21 ± 0.01 for IGF1R ECD-TM-fp without IGF1 or 0.34 ± 0.02 for with IGF1, 0.36 ± 0.02 for IGF1R ECD-ΔL1-TM-fp and 0.38 ± 0.02 for IGF1R ECD-TM-fp H905C.

Figure 2.5. IGF1R TMs associate

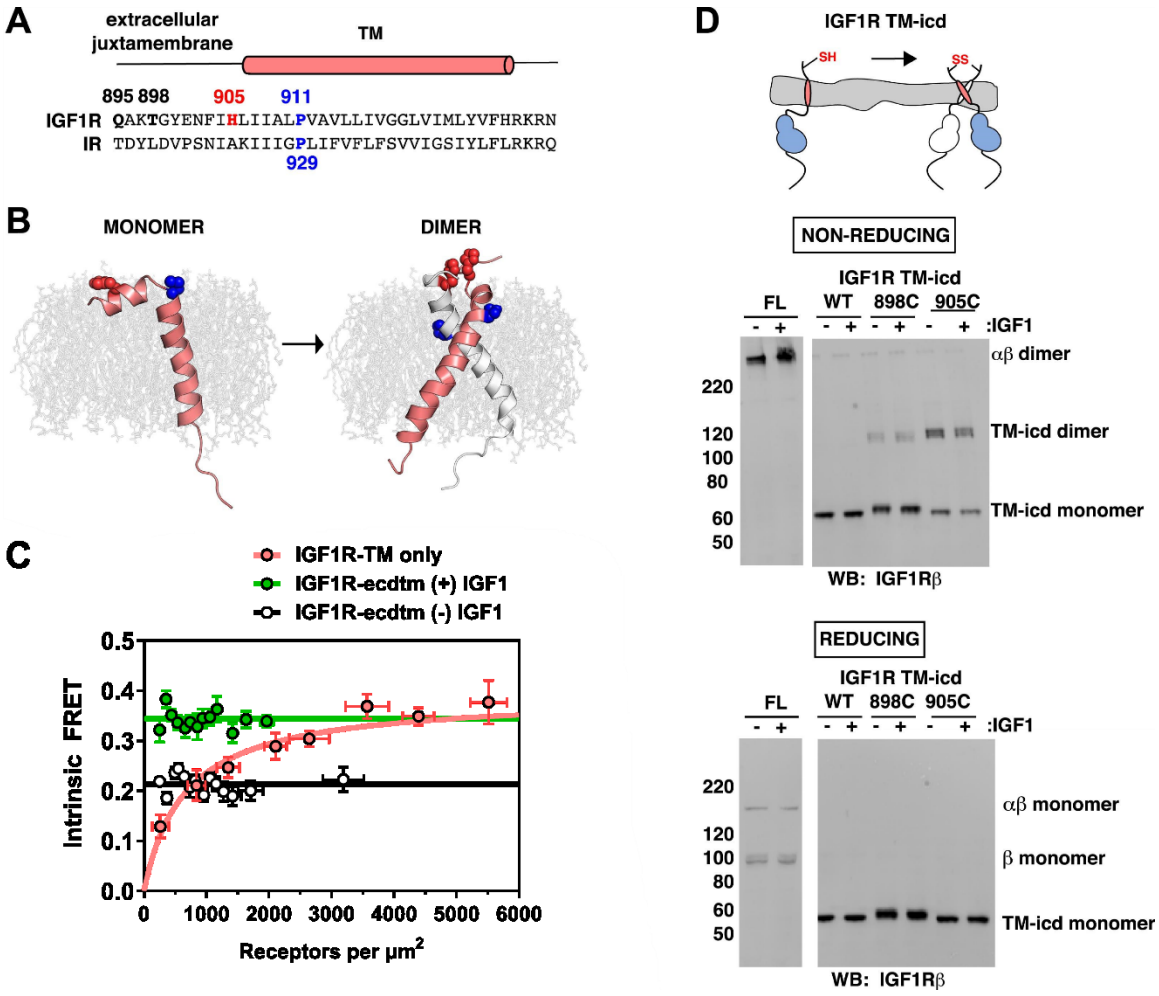

Figure 2.5. (**A**) Sequence alignment of human IGF1R and IR extracellular juxtamembrane and TM regions. The position of the TM is indicated above the alignment. Bold lettering highlights residues targeted for substitution. H905 (red) and P911 (blue) are colored. (**B**) IGF1R TM monomer and dimer structures observed in MD simulations are shown in ribbon (white and pink). Shown in spheres are P911 (blue) and H905 (red). The lipid bilayer is in light gray. (**C**) The intrinsic FRET efficiency for IGF1R TM-fp plotted (pink) as a function of TM concentration. Also shown for reference

is IGF1R ECD-TM-fp in the presence (green) or absence (white) of ligand. Each data point represents the binned average of at least eight vesicles (±s.e.m. in both x and y). For IGF1R TM-fp, the data were fit to a two state association model with a peak value of 0.38 ± 0.02. (**D**) Cartoon of IGF1R TM-icd with the positions of single-site cysteine mutations indicated in red (top). Anti-IGF1Rβ Western blots of lysates of HEK293 cells expressing either IGF1R-fl or IGF1R TM-icd fragments (WT, 898C or 905C) incubated with or without IGF1 and analyzed on non-reducing (middle) or reducing gels (bottom).

Figure 2.6. TMs associate in active IGF1R-fl

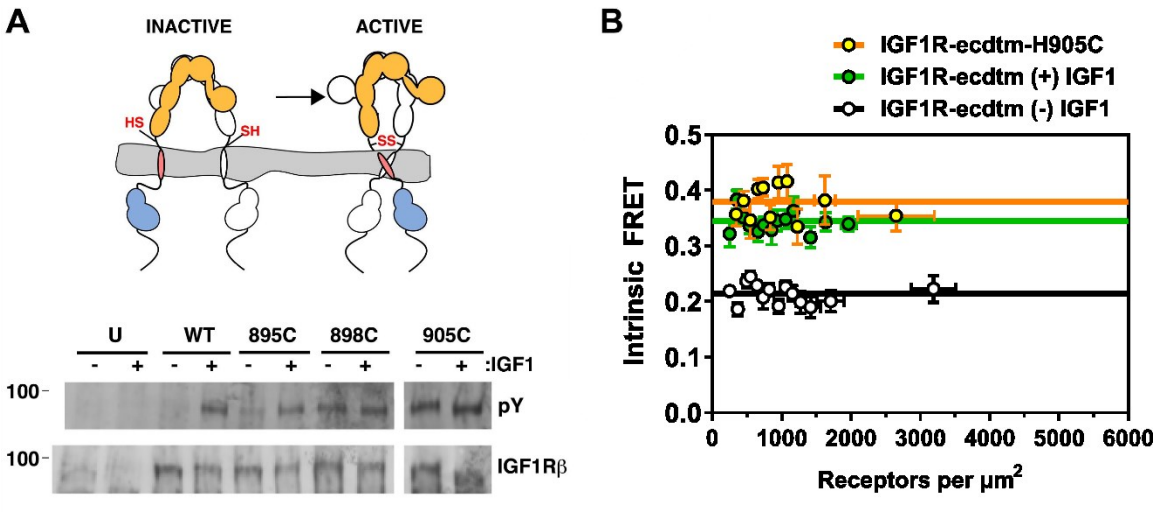

(**A**) Cartoon of IGF1R-fl with cysteine substitutions (top). Western blots of immunoprecipitated normalized cell-lysates from untransfected cells (U) or cells transfected with IGF1R-fl (WT) or IGF1R-fl proteins with cysteine substitutions (895C, 898C, or 905C) incubated the presence or absence of IGF1 (bottom). All panels are from the same blot. (**B**) Plot of the intrinsic FRET efficiency of IGF1R ECD-TM-fp with the H905C substitution (yellow) and fit to a horizontal line with a value of 0.38 ± 0.02. Each data point represents the binned average of at least eight vesicles (±s.e.m. in both x and y). For reference, the intrinsic FRET efficiencies and fits for IGF1R ECD-TM-fp with ligand (green) or without ligand (white) are also shown.

Figure 2.7. Model of IGF1R activation

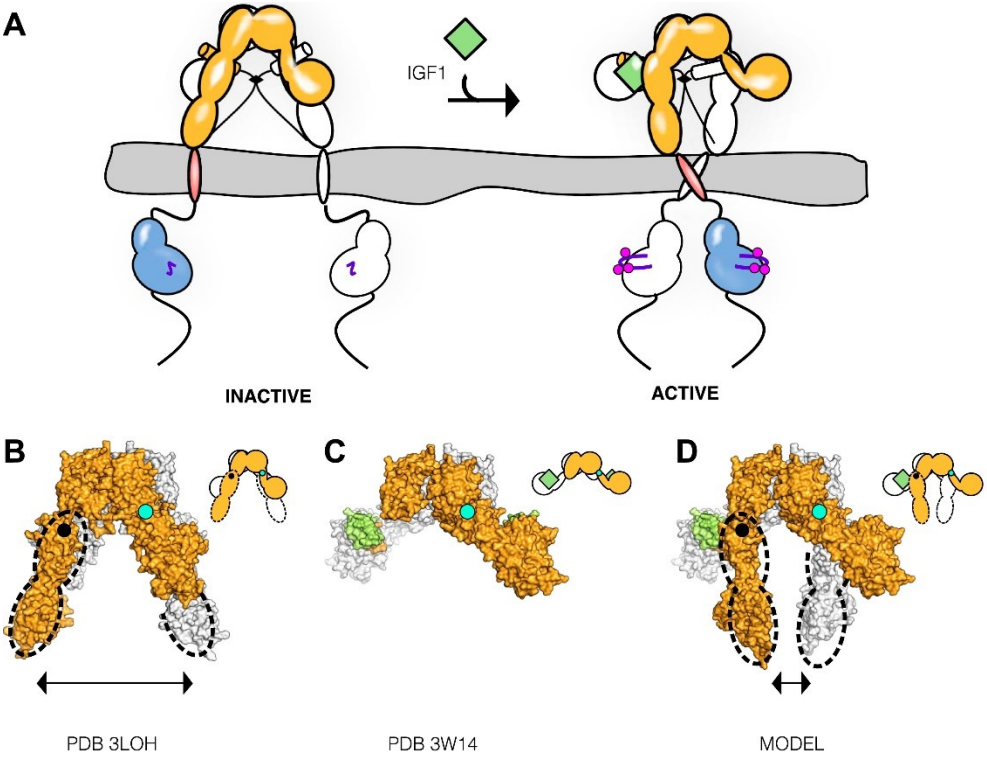

Figure 2.7. (**A**) Cartoon model of IR family activation. The IDs are shown as black lines in the ECDs, the disulfide linkages as black diamonds, phosphorylation as pink circles, activation loops as purple lines, ligand as green diamonds, and αCTs as cylinders. Surface representations and corresponding cartoon diagrams of (**B**) the ECD of unliganded-IR (PDB 3LOH; Smith et al., 2010), (**C**) insulin bound to the IR ECD fragment (PDB 3W14; Menting et al., 2013), or (**D**) a model of the entire IR ECD bound to two Insulin molecules. For each panel, one αβ subunit is colored white and the other orange, and Insulin green. Dashed lines outline the Fn2-3 domain tandems. The hinge point between F1 and Fn2-3 domains is indicated by black circles and cyan circles indicate the hinge point between CR and L2 domains.

Chapter 3: The ErbB1 and ErbB2 intracellular domains promote ligand-independent dimer formation

Acknowledgements

Matt Ward provided helpful advice and technical assistance during the early stages of this project. Thanks to Rachel Green and her laboratory for the use of their Typhoon imaging system, and to Andrew Goodrich and Jennifer Kavran for critical reading of the early manuscript. Sarvenaz Sarabipour and Nuala Del Piccolo provided essential assistance and advice when performing FRET microscopy, and Lily Raines provided purified EGF.

Introduction

Human epidermal growth factor receptor EGFR/ErbB1 and its homolog, HER2/ErbB2, play important roles in both health and disease. While both are essential for normal growth and development, abnormal activation of either promotes the progression of glioblastoma, non-small cell lung cancer, and breast cancer. ErbB1 and ErbB2 are integral membrane proteins composed of an extracellular domain (ECD), a single transmembrane alpha-helix, and an intracellular domain (ICD). The ICD comprises a juxtamembrane region, a tyrosine kinase domain and a ~230 amino acid c-terminal tail of unknown structure. Several decades of research have established that ErbB1 functions by a mechanism of ligand-dependent activation. Binding of epidermal growth factor

(EGF) or several of its homologs to the ECD promotes ErbB1 dimer formation and stimulates tyrosine kinase activity.

Many experiments indicate that a fraction of cell-surface ErbB1 is dimeric in the absence of ligand (Macdonald & Pike, 2008) (Liu, et al., 2007) (Nagy, et al., 2010) (Saffarian, et al., 2007) (Chung, et al., 2010), which suggests free ErbB1 exists in equilibrium between monomers and dimers. Despite considerable progress, the nature and strength of ligand-independent ErbB1 dimers remains elusive, as estimates of the fraction of ligand-independent dimers range from 14-75% (Table 3.1). The high variance may be explained in part by the variety of experimental techniques, cellular contexts, and reported ErbB1 expression levels present in different studies (Table 3.1). Further uncertainty stems from an incomplete understanding of the nature and signaling competence of the unliganded ErbB1 dimer. In particular, the relative contributions of each domain in mediating ligand-independent dimer formation remain unclear.

A complete model for the mechanism of ErbB1 activation requires understanding how the receptor maintains itself in an inactive state when not bound to ligand. On this point, the principal functions of each domain are known to varying degrees. In the absence of ligand, the ECD adopts a tethered conformation that may play a role in receptor autoinhibition (Cho & Leahy, 2002) (Ferguson, et al., 2003) (Bouyain, et al., 2005) (Endres, et al., 2013). Binding of EGF to the ECD promotes an extended conformation, which exposes an extended β-hairpin (termed the 'dimerization arm') that mediates the active receptor dimer. Disrupting the intradomain tether fails to activate the receptor (reference needed), but mutating residues within the dimerization arm ligand-

induced inhibits receptor activation (Ogiso et al. 2002, Garrett et al. 2002). The precise mechanism by which the ECD achieves autoinhibition thus remains an area of intense research (Bessman, et al., 2014) (Lee, et al., 2015). Comparatively little is known about the inactive state of the TM domain or ICD, though a mechanism by which the TM may function in the inactive state has been proposed (Endres, et al., 2013) (Arkhipov, et al., 2013) (Ben Tal et al., 2002).

What then are the determinants of ligand-independent association, what are the barriers to the formation of the active state, and how does ligand binding overcome them? To address these issues, we present quantitative Forster resonance energy transfer (FRET) measurements of ErbB1 and ErbB2 interactions in vesicles derived from plasma membranes. We show that the transmembrane (TM) domains of EGFR and ErbB2 have an intrinsic propensity to form homo- and hetero-dimers. The ECDs disrupt intrinsic TM interactions, while the intracellular domains promote dimer formation in the absence of ligand. Mutations in the asymmetric dimer interface important for kinase activation do not affect the formation of ligand-independent dimers. ErbB receptors form dimers as a function of membrane surface concentration, and the two-dimensional dissociation constant falls within the known range of physiological expression. These results implicate the ICD as a driver of dimer formation in the absence of ligand and suggest that inactive, ligand-independent ErbB1 dimers may utilize an interface that is distinct from the asymmetric kinase dimer observed in the active conformation.

Results

Quantitative Imaging FRET Microscopy

We generated variants of ErbB1 and ErbB2 with either a FRET donor (EYFP) or acceptor (mCherry) fused to the C-terminus (Fig. 3.1A). Each ErbB-FP (FP: fluorescent protein) fusion protein was activated in a ligand-dependent manner in CHO cells (Fig. 3.1B). We then employed quantitative imaging FRET (QI-FRET) microscopy, a method that permits measurements of protein-protein interactions in plasma-membrane vesicles formed by exposing cells to high salt concentrations. The details of the method have been described in detail elsewhere (Li, et al., 2008) (Chen, et al., 2010a) (Chen, et al., 2010b). Briefly, receptor variants fused separately to EYFP or mCherry were transiently co-transfected into CHO cells, resulting in a wide range of expression in a single experiment. The dimerization-impaired A206K variant of EYFP was used, which reduces the solution EYFP dimerization constant from 111 μM to 74 mM (Zacharias, et al., 2002). The FRET efficiency was measured in CHO cell plasma membrane-derived vesicles, referred to hereafter simply as "vesicles" (Fig. 3.6). EGF-dependent receptor activity was preserved in vesicles generated from A431 cells, which express ErbB1 endogenously (Fig 3.6B). Each experiment yields the measured FRET efficiency as a function of concentration (Fig. 3.6C). We then calculate the 'corrected FRET', which accounts for contributions due to interactions resulting from random proximity as well as different ratios of donor and acceptor molecules in each vesicle.

The efficiency of resonance energy transfer between fluorescent donor and acceptor molecules depends on both the relative orientation and distance separation between the two respective transition dipole moments (Lakowicz, 2006). To mitigate any effects of orientation of the FPs on FRET measurements, we included a flexible 8-amino acid linker sequence between each receptor variant and its FP fusion partner. We assume any changes in FRET mostly reflect changes in distance separation. For the case of the receptor-receptor interactions studied here, we interpreted concentration-dependent FRET changes as resulting from a change in oligomeric state. Conversely, FRET values that did not change with 2D-concentration were assumed to represent a single oligomeric state. Where appropriate, we fit the data to a monomer-dimer equilibrium model which includes to parameters: 1) the 'intrinsic FRET', $\tilde{E}$, which equals the FRET efficiency within a dimer and 2) the two-dimensional (2D) dissociation constant, K, in units of molecules/μm^2 (cite pertinent Hristova FRET papers). In cases where the association was too strong to determine, we assumed the intrinsic FRET value ($\tilde{E}$) was to equal the mean of the distribution over all concentrations.

The ErbB1 and ErbB2 TM domains form homo- and hetero-dimers in membrane-derived vesicles

The single TM domains of ErbB1 and ErbB2 are known to associate in bacterial membranes (Mendrola, et al., 2002). To investigate the strength of these interactions, we measured the FRET efficiency as a function of 2D-membrane concentration (molecules/μm^2) for three interaction pairs in CHO vesicles: (i) the homodimer of ErbB1-TM-fp, (ii) the homodimer of ErbB2-TM-fp, and (iii) the heterodimer of ErbB1-TM-fp

and ErbB2-TM-fp. These receptor variants consisted of the transmembrane domains linked to a fluorescent protein (Fig. 3.1; pink circles in Fig. 3A-C). We could not determine the dimer dissociation constants for each of the three pairwise interactions, which likely fall too far below the sensitivity limit of the experiment (about 200 molecules/μm^2). The FRET efficiency changed little with concentration, and the mean for each population was ~0.35. Within the membrane environment of the vesicle, the isolated TM domains therefore showed a strong propensity to form dimers in the absence of the extracellular and intracellular domains.

ErbB extracellular domains inhibit intrinsic transmembrane (TM) domain interactions

Since the ErbB ECDs are known to function in an autoinhibitory manner (McManus, et al., 1997) (Boerner, et al., 2000) (Ferguson, et al., 2003) (Bouyain, et al., 2005) (Cho & Leahy, 2002) (Endres, et al., 2013), we investigated the effect of the ECDs on the TM domain association. In the absence of ligand, the FRET efficiency decreased for receptor variants that include both the ECD and TM domains (Fig. 3.2) relative to the FRET measured for the TM domains alone (Fig. 3.2A-C, compare pink and grey circles). ErbB1-ECDTM-fp alone showed low (<0.1) FRET efficiency at concentrations below 1000 molecules per μm^2, with FRET efficiency increasing modestly to ~0.2 at receptor concentration levels of 3000 per μm^2 (Fig. 2A). In a similar manner, the FRET efficiency for ErbB2-ECDTM-fp stayed below 0.2 over all receptor concentrations measured (Fig. 3.2C). We were unable to reliably fit the data for homo-interactions of either ErbB1 or ErbB2 to a monomer-dimer equilibrium. In contrast to the homodimer cases, unliganded heterodimers of ErbB1-ECDTM-fp and ErbB2-ECDTM-fp formed at relatively low

receptor concentration in the absence of ligand (Fig. 3.2C). The best fit value for the dimer dissociation constant was 704 molecules/μm^2.

We then measured the FRET efficiency as a function of receptor concentration for these variants (ECD-TM) in the presence and absence of EGF (Fig. 3.2A and Fig. 3.2C). Binding to EGF led to an increase in FRET efficiency for homodimers of ErbB1-ECDTM-fp (Fig. 3.2A, $\tilde{E} = 0.39$) and heterodimers of ErbB1-ECDTM-fp and ErbB2-ECDTM-fp (Fig 3.2C, $\tilde{E} = 0.39$) for all observed receptor concentrations. In agreement with similar experiments using luciferase-fragment complementation (Macdonald-Obermann, et al., 2012) these data indicate that: i) EGF binding to the ECD of ErbB1-ECDTM-fp promotes dimer formation, and ii) the TM domains come into close proximity within this dimer. For all ligand-independent interactions, the 95% confidence intervals for both model parameters were large (K and $\tilde{E}$; 95% CI $\geq$ mean). It is therefore difficult to distinguish between a very weak dimer with high intrinsic FRET and a stronger dimer with low intrinsic FRET, though in either case the ECD effectively separates the TM domains.

To examine the FRET efficiency for a constitutively dimeric control protein, we replaced the ECD of ErbB1-ECDTM-fp with the mouse immunoglobulin Fc-region. Since the mouse IgG-Fc is constitutively dimeric, we reasoned that fusing it to the N-terminus of the ErbB1 TM region would result in a strong dimer with high FRET (Bessman, et al., 2014). Indeed, the measured FRET efficiency for Fc-ErbB1-TM-fp was high ($\tilde{E} = 0.43$) and showed no change with concentration, consistent with the expected FRET for a constitutive dimer in which the TM domains are in close proximity (Fig. 3.7).

Importantly, the data overlay closely with the measured FRET for ErbB1-ECDTM-fp in the presence of saturating EGF, suggesting that the ErbB1-ECDTM-fp population in this condition is mostly dimeric.

The ErbB intracellular domains promote dimer formation in the absence of ligand

Our results indicate that ErbB TM domains associate on their own, but that ECDs counteract this effect. We then examined the relative contribution of the intracellular domain (ICD) to ligand-independent dimer formation. Preliminary experiments using full-length variants of ErbB1 and ErbB2 with fluorescent proteins fused to the C-terminus were inconclusive. The total membrane expression of these variants was below 200 molecules/μm^2, though expression and activity were detectable by western blot (data not shown). Removal of 107 and 25 amino acids from the C-termini of ErbB1 and ErbB2, respectively, resulted in variants that increased membrane surface expression by about 5-fold. These truncations do not impair ligand-dependent activity (Fig. 3.1B).

For all pairwise near full length ErbB-fp interactions measured, we observed that the ICDs promote dimer formation in the absence of ligand (Fig. 3.3). We detected a concentration-dependent increase formation in FRET efficiency for homodimers of ErbB1-Δ107-fp, with a best fit value for the 2D dimer dissociation constant (K_d) of 146 molecules/μm^2 (Table S1). Homodimers ErbB2-Δ25-fp and heterodimers of ErbB1-Δ107-fp and ErbB2-Δ25-fp interacted strongly: the FRET efficiency was high (~0.4) and remained fairly constant with increasing concentration, consistent with the behavior for a constitutive dimer. Addition of EGF led to an increase in FRET for the homodimer of ErbB1-Δ107-fp. The FRET efficiency remained constant (~0.35) over all concentration

range, and the intrinsic FRET (Ẽ) was not statistically different between ligand-independent and EGF-bound ErbB dimers. Ligand binding thus increases the oligomerization propensity of near full length ErbB-fp variants, while the average distance between the fluorescent dipoles for ligand-independent and EGF-bound dimers (or oligomers) is similar.

EGF-independent ErbB1 phosphorylation increases with increasing receptor surface density

Gene amplification of ErbB1 and ErbB2 is associated with the genesis and progression of subsets of glioblastoma and breast cancers, respectively (Ekstrand et al., 1991) (Slamon et al., 1989). Increased ErbB1 cell surface expression results in ligand-independent receptor phosphorylation at tyrosine-1068 (Endres, et al., 2013) (Valley et al., 2015), which implies that some fraction of unliganded dimers samples the active state. To further examine the relationship between dimerization and activation, we generated a panel of CHO cell lines stably expressing full length ErbB1 fused to EYFP at the C-terminus (ErbB1-EYFP). The apparent ErbB1-EYFP surface concentration was measured in vesicles derived from each cell line and ranged from <100-300 receptors per μm^2 on average (Fig. 3.4A and Fig. 3.8). Cells treated with and without EGF were analyzed by western blot for ErbB1 and pTyr (Fig. 3.4A-C). In the absence of ligand, ErbB1 phosphorylation was not detectable at concentration levels below 100 molecules/μm^2. Between 100 and 300 molecules/μm^2, ligand-independent phosphorylation increased in a linear fashion. Stimulation with EGF results in a steady linear increase in phosphorylation across all measured expression levels (Fig. 3.4C).

Interestingly, the ErbB1-EYFP expression range over which EGF-independent phosphorylation begins to rise (100-300 molecules/μm^2) agrees closely with the best fit value for the 2D-dissociation constant for ErbB1 (146 molecules/μm^2). Together, these data suggest that surface density-dependent dimerization might underlie ligand-independent activation.

We also examined the influence of ErbB1 overexpression on two downstream signaling pathways: STAT and MAPK/Erk (Fig. 4A). Increased expression of ErbB1 had no measurable effect on Erk1/2 phosphorylation in the absence and presence of EGF, nor did it alter or Erk1/2 expression. The total STAT1 expression levels and the increased modestly (about 2 fold) with increasing ErbB1 expression. Interestingly, the level of EGF-dependent pSTAT1 was enhanced in ErbB1-YFP overexpressing cells (Fig. 3.4, Fig. 3.9). We did not observe background phosphorylation of either STAT1 or Erk1/2 in any of the CHO ErbB1-YFP cell lines, regardless of ErbB1 expression level.

Disrupting the asymmetric dimer interface does not impair ligand-independent dimer formation

A key feature of activated ErbB1 dimers is the formation of an asymmetric interface between kinase domains within a dimer, termed the “asymmetric kinase dimer”. Two single-residue substitutions at this interface, one located in the kinase N-lobe (I682Q), the other in the C-lobe (V924R), each themselves abolish ErbB1 activity. Co-expression of ErbB1-I682Q with ErbB1-V924R restores ligand-dependent activity (Zhang, et al., 2006) (Fig. 3.5A). Since ligand-independent dimers can undergo

phosphorylation, we wondered if the asymmetric kinase interface might also mediate the formation of unliganded ErbB1 dimers.

Despite evidence that unliganded dimers possess some intrinsic activity (Fig. 3.4) (Valley et al., 2015) (Endres, et al., 2013), we observed that disrupting the asymmetric dimer interface does not affect formation of ligand-independent ErbB1 dimers (Fig. 3.5). We introduced the I682Q and V924R mutations into the ErbB1-Δ107-fp variant, then measured the dimerization propensity of each with our FRET assay in vesicles. Neither variant had a strong effect on the propensity for ErbB1 to form ligand-independent dimers. In the absence of EGF, the dimerization coefficients for the I682Q and V924R variants were 209 and 178 molecules/μm^2 (Fig. 3.5B-C), which do not differ significantly from the value determined for the wildtype receptor.

The kinase-activating L834R mutation promotes ligand-independent ErbB1 self-association

Two ErbB1 variants associated with lung cancer (L834R and Δ722–726) are located within the ErbB1 kinase domain. Both induce ligand-independent receptor activity, in part because they enhance the propensity for ErbB1 to form active dimers (Zhang, et al., 2007) (Shan et al., 2012) (Valley et al., 2015). To investigate the effect of a kinase-activating mutation on the strength of ErbB1 self-interactions, we introduced the L834R mutation to ErbB1-Δ107-fp and measured its FRET efficiency in membranes. $ErbB1_{L834R}$-Δ107-fp showed high FRET over all concentration ranges measured, indicating that this variant forms strong dimers (Fig. 3.3A, purple circles). Furthermore, the FRET efficiency profile overlays closely with ErbB1-Δ107-fp in the presence of

EGF, which suggests that the L834R variant favors the formation of the asymmetric kinase and the active state.

Discussion

While many previous studies have documented the occurrence of preformed ErbB1 dimers, none to our knowledge have determined the strength of the interaction. Several research groups have estimated of the strength of ligand-independent dimer by determining the expression level of the cell line under study (Table 3.1). While informative, these measurements are limited in one important respect: each is derived from a population of cells. Since the distribution of ErbB1 expression may vary 10-100 fold even within a monoclonal cell line population, any estimates of the fraction of dimers will necessarily represent the population average. Furthermore, these studies measured expression levels in numbers of molecules per cell, which makes limiting assumptions about the complex topology of the membrane.

To overcome these limitations, we used QI-FRET, a method that enables direct observation of dimer formation between ErbB-fp variants embedded in membrane vesicles. For each individual vesicle in a population, we experimentally determined both the FRET efficiency and the 2D membrane concentration. QI-FRET also accounts for the effect of stochastic interactions that result from increased concentration in the 2D-membrane environment (King, et al., 2016), which provides for clear identification of *bona fide* protein interactions. This allowed us to assess the contributions of each domain to dimer formation in a systematic, quantitative manner.

ErbB-fp variants composed of the TM domains alone form strong dimers in membrane vesicles. This appears to be a feature of all human receptor tyrosine kinase TM domains (Finger, et al., 2009). In contrast, variants composed of both the ECD and TM domains exhibit reduced association (Fig. 3.2). The ECD thus acts as a barrier to TM region association. Interestingly, neither the unliganded ErbB1 ECD nor the TM domains form dimers in solution (Lemmon, et al., 1997) (Stanley & Fleming, 2005). Restriction to the plasma membrane must therefore promote TM dimerization, likely due to increased local concentrations and a reduction in translational and rotational degrees of freedom in going from a 3D solution into the 2D membrane (Lin, et al., 2014). In contrast, an autoinhibitory role for the ganglioside GM3 on ErbB1 activation has been observed by others (Coskun, et al., 2011). The plasma membrane-derived vesicles used in our experiments do contain a fraction of GM3 (1-2 mole %), though we did not examine the effect of GM3 on ErbB1 dimer formation in our experiments (Sarabipour, et al., 2015). It is clear that the role of the membrane in regulating ErbB oligomer formation warrants further investigation.

Our results identify the ICD as a critical mediator of ligand-independent dimers (Fig. 3.3), consistent with implications from previous experiments. Deleting the ErbB1 ICD leads to a decrease in ligand-independent receptor crosslinking in cells (Yu, et al., 2002) , as well as a loss of negative cooperativity in binding to EGF (Macdonald & Pike, 2008). Furthermore, our experiments concur qualitatively with single molecule observations of ErbB1 in cell membranes. Measurement of average ErbB1 dimer lifetimes (t_D) revealed that deleting either the dimerization arm (t_D = 9.7 ± 0.9 seconds) or

the intracellular domain (t_D = 4.5 ± 0.1 s) reduced the dimer lifetime relative to wildtype (t_D = 13.0 ± 1.2 s) (Chung, et al., 2010).

Our interpretation of the 2D-dissociation constants is necessarily limited, since we lack a complete understanding of the ErbB1 surface concentration levels under various physiological conditions. Expression levels are typically reported as the average number of receptor molecules/cell, whereas our measurements are in units of molecules/μm^2. Caution should be taken when converting between these two units of measure, since doing so requires making simplifying assumptions about the geometry of the plasma membrane. We can nevertheless estimate that the best fit 2D-dissociation constant we measured for ligand-independent ErbB1 dimers (Table S1) corresponds to ~140,000 receptors/cell, assuming a radius of 9 μm and spherical geometry for a CHO cell (Fig. 3.8). This figure falls well within the range of ligand-independent ErbB1 dimeric fractions reported in the literature (Table 3.1). A recent study reported the surface expression levels in A431 cells (646 molecules/μm^2), which again places the observed K_D for preformed ErbB1 dimers in the range of intermediate expression (Zhang et al, 2015). Thus under conditions of low expression (~10,000 receptors/cell) we estimate that the receptor is only ~10% dimeric, whereas oligomers dominate at high expression levels (~70% dimer fraction at 500,000 receptors/cell).

In ErbB1-YFP overexpressing cells, the total amplitude of EGF-independent ErbB1 phosphorylation is roughly equal to the amplitude of EGF-dependent phosphorylation in low-expressing cells (Fig. 3.4, compare lanes 1-2 to lanes 11-12). Nevertheless, ligand-independent ErbB1 phosphorylation does not result in a concomitant

phosphorylation of either Erk1/2 or STAT1, although STAT1 expression does increase modestly (but not Erk1/2). However, any interpretation of protein expression levels measured in our western blot experiments should be taken with caution, due the >10-fold variation in expression levels within each stable cell line (Fig. 3.4A). Furthermore, regulation of ErbB1 downstream signaling involves a complex network of feedback and feedforward loops (Avraham & Yarden, 2011), and such mechanisms will likely influence state of ligand-independent ErbB1, STAT, and Erk phosphorylation. Indeed, ErbB1 undergoes rapid phosphotyosine (p-Tyr) turnover, indicating that phosphatases exert continual control over phosphorylation levels (Kleiman, 2011). Furthermore, pre-treatment of ErbB1-expressing cells with orthovanadate, a pan-phosphotyrosine phosphatase inhibitor, results in enhanced EGF-dependent ErbB1 activation (Lahusen, et al., 2007) (Reddy, et al., 2016). The total level of ErbB1 phosphorylation will therefore depend on the two competing ErbB-kinase and phosphatase activities.

How are ligand-independent dimers kept in a low-activity state?

The different regions of ErbB receptors (ECD, TM and ICD) function together to regulate dimer formation. The ECD plays a dual role, inhibiting dimerization in the absence of ligand and facilitating dimerization when ligand is bound. On the other hand, both the TM and the ICD appear to promote dimer formation (Figs 3.2, 3.3). Near full length ErbB1-fp can form ligand-independent dimers even if the asymmetric interface is disrupted by mutations (Fig. 3.5B-C). At the same time, the V924R and I682Q variants do not lead to ligand-independent activity (Fig. 3.5A), which suggests that some other interface may be responsible for the association we observed. ErbB1-V924R cannot form

the asymmetric kinase dimer when bound to EGF, though the kinase domain does appear make symmetric contacts under these conditions (Mi, et al., 2011). The inactive form of the kinase domain has also been observed to make symmetric contacts within a crystal. In any case, the ligand-independent and ligand-dependent ErbB dimers are indistinguishable in our FRET experiments (Fig. 3.3), though whether or not this reflects a true similarity in the kinase domain configuration between the two types of dimers is unclear. Our choice of large (27kDa) genetically-encoded FPs (EYFP and mCherry) necessarily restricted the placement of fluorescent probes to either the C-terminal ends of receptor variants, thereby limiting our capacity to interrogate conformational movements at precise locations within the ICD. Future experiments will be needed to determine the manner in which the ICD participates in non-asymmetric dimer contacts.

The ECD also plays a crucial role in ErbB1 autoinhibition, though the mechanism of action remains obscure. Our results show that while the ECDs may reduce the interaction between the TM domains, they do not preclude dimer formation altogether (Fig. 3.2). Our experiments cannot address the precise structural nature of the unliganded ECDTM homodimers, since the data did not fit well to a monomer-dimer equilibrium. The ErbB1-ECDTM variants conforms to one of two possible models: either this variant forms 1) weak ligand-independent dimers that exhibit a similar degree of TM separation as the EGF-bound form, ($K>3000$ molecules/μm^2, $\tilde{E} \approx 0.4$) or 2) strong dimers that exhibit a greater degree of TM separation than the ligand-bound form ($K<500$ molecules/μm^2, $\tilde{E} \approx 0.4$). Of the known structures of the ErbB1 ECD, the tethered conformation seems likely to preclude TM interactions, presumably by steric occlusion.

The fact that we still observe receptor self-association in the ECDTM variants suggests that some fraction of unliganded receptors can sample the extended conformation. In that case, the relative probabilities of each state (tethered vs. extended) would likely determine how often the TM domains are able to interact. Of course, since the ensemble nature of our FRET assay reports on the average conformation within a population of receptors, we cannot rule out that the ECDs might adopt some other conformation that holds the TM domains apart in space. Consistent with this idea, a chimeric receptor composed of the insulin receptor (IR) ECD and the ErbB1 TM domain and ICD becomes activated in response to insulin binding (Reidel, et al., 1986), implying that ErbB1 and insulin receptor may share a common mechanism. The insulin/insulin-like growth factor receptor (IR/IGF1R) family involves TM domain spatial separation in the inactive state (McKern et al., 2006) (Kavran, et al., 2014).

A different mode of regulation within ligand-independent dimers been proposed by others, one in which kinase activity appears coupled to slight conformational changes within dimerized TM domains (Maruyama, 2015) (Endres, et al., 2013) (Arkhipov, et al., 2013). Changes to the TM dimer conformation may include TM domain rotation, or conformational switching between two GxxxG-like motifs located in the N- and C-terminal regions of the TM domain. Neither model need exclude the other: both the separation of the TM domains (implied by our experiments) and the conformational switching between the GxxxG-like motifs (proposed by others) might each represent discrete steps along the path from inactive monomer to active dimer. Finally, the kinase-proximal region of the C-terminal tail has also been implicated in negative regulation

(Pines, et al., 2010) (Kovacs, et al., 2015). A full understanding of the relative contributions of these proposed modes of regulation will require further investigation of intact receptors in the membrane environment.

Materials and Methods

Plasmid Construction

The coding sequences for ErbB1, ErbB2, EYFP and mCherry were amplified using the polymerase chain reaction and cloned into pCDNA3.1(+) (*Life Technologies*). The sequence for EYFP was modified using site directed mutagenesis to generate the EYFP A206K variant.

Cell culture and transfection

Chinese hamster ovary (CHO) cells and A431 cells were maintained in Dulbecco's modified Eagle Medium (DMEM F12) supplemented with 2 mM glutamine, 5% FBS and grown at 37 °C, 5% CO_2. For imaging experiments, CHO cells were seeded in 35 mm dishes at a density of 2 x 10^4 cells per well, then grown for 24 hours prior to transfection. We used the Lipofectamine 3000 transfection reagent (*Life Technologies*) according to the manufacturer's protocol.

Vesiculation, Image Acquisition and Analysis

All vesiculation procedures were performed as described (Kavran, et al., 2014). For ligand addition experiments, EGF was added to the vesicles to a final concentration

of 100 nM and incubated for at least 1 hour prior to imaging. Vesicle images were acquired using a Nikon C1 laser scanning confocal microscope at 60X magnification (water immersion objective). For each vesicle, three scans were recorded: a 'donor' scan (λ_{exc} = 488 nm, λ_{em} = 500-530 nm), an 'acceptor' scan (λ_{exc} = 543 nm, λ_{em} = 650 nm longpass), and a 'FRET' scan (λ_{exc} = 488 nm, λ_{em} = 565-615 nm). Argon (488 nm) and He-Ne lasers were used as excitation sources. The image pixel dimensions were 512 x 512, and the pixel dwell time was 1.68 μs, and the gains were set to 8. The Förster radius for the EYFP-mCherry pair was calculated to be 53.1 Å. All images were processed using a MATLAB program written in the Hristova laboratory which calculates the FRET efficiency for each vesicle. A detailed description of the analysis is found elsewhere (Chen, et al., 2010a) (Chen, et al., 2010b). Absolute protein concentration in the membrane was calculated by comparing the fluorescence intensity in vesicles with the intensities measured from a dilution series of fluorescent protein standards (EYFP and mCherry). Bleed-through coefficients were calculated for each experiment (typically ~0.3 and ~0.2 for EYFP and mCherry, respectively). Where appropriate, the processed data (FRET vs. concentration) were fit to a monomer-dimer equilibrium model using Graphpad Prism:

$$X_{\mathrm{d}} = \frac{1}{8}\left(K_{\mathrm{d}} + 4X_{tot} - \sqrt{K_{\mathrm{d}}(K_{\mathrm{d}} + 8X_{\mathrm{tot}})}\right)$$

where X_d is the fraction of dimers, K_d is the dissociation constant, and X_{tot} is the total concentration of receptor:

$$X_{\text{tot}} = X_{\text{monomer}} + 2(X_{\text{dimer}}).$$

EGF Stimulation of ErbB proteins in CHO cells

EGF was expressed in *E. coli* and purified as described (Qiu et al, 2009). CHO cells were grown to 90% confluency, then transfected and grown for 14 hours, then serum starved for 7 hours at 37 °C in Ham's F12 supplemented with 1 mg/mL BSA. The cells were incubated in starvation media in the presence or absence of 100 nM EGF (5 minutes, 37 °C). The medium was aspirated, the cells were washed twice with cold PBS (1X, plus 1 mM Na_3VO_4), then lysed for 15-20 minutes at room temperature in RIPA buffer (150 mM NaCl, 50 mM Tris pH 8, 1% NP40, 0.5% w/v sodium deoxycholate, 0.1% sodium dodecyl sulfate, 1 mM Na_3VO_4). The lysates were clarified by centrifugation and the total protein concentration of the supernatants was determined by BCA assay (*Pierce, Life Technologies*). Lysate protein concentrations were normalized, and the samples were analyzed by SDS-PAGE and western blot to detect phosphotyrosine (4G10, *Millipore*), ErbB1 (D38B1) ErbB1 pY1068, ErbB2 (29D8), or ErbB2-pY1221/1222 (all ErbB antibodies purchased from *Cell Signaling Technology*).

Figure 3.1 ErbB1 and ErbB2 tagged with fluorescent proteins are active in CHO

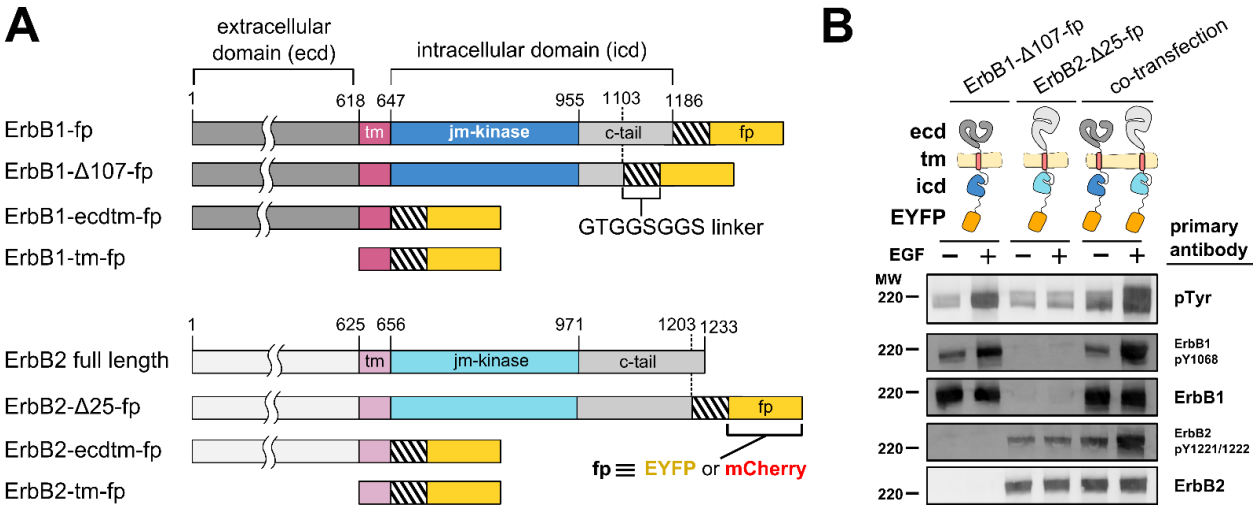

Figure 3.1. ErbB1 and ErbB2 tagged with fluorescent proteins are active in CHO cells (A) Schematic representation of fluorescent protein (fp)-tagged variants of ErbB1 and ErbB2. Abbreviations: ecd, extracellular domain; tm, transmembrane domain; icd, intracellular domain; jm, juxtamembrane; fp, fluorescent protein. Residue numbers are indicated above the full length proteins. The numbering convention is for the mature proteins and does not include the signal sequence for ErbB1 or ErbB2. (B) Western blots of CHO cell lysates with or without EGF stimulation, expressing either ErbB1-Δ107-YFP, ErbB2-Δ25-YFP, or both. Primary antibodies are indicated next to each image. Blots are representative of three independent experiments.

Figure 3.2. The ECDs impede intrinsic TM interactions, and ligand binding releases the constraint

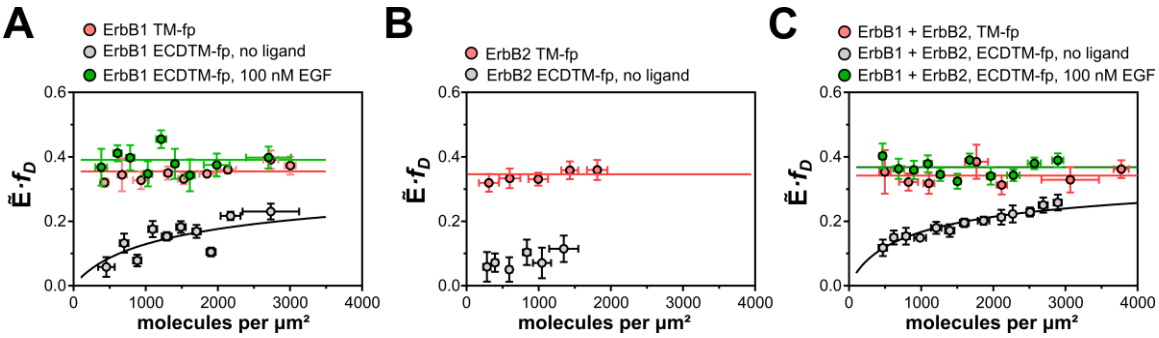

Figure 3.2. Corrected FRET efficiency as a function of total receptor membrane concentration for ErbB-TM-fp and ErbB-ECDTM variants. (A) ErbB1 homo-interactions, (B) ErbB2 homo-interactions and (C) ErbB1 and ErbB2 hetero-interactions. In each plot, variants comprising the TM domain alone are shown in pink, while variants comprising the ECD + TM domains are shown in grey (no ligand) and green (100 nM EGF). Data in the absence of ligand were fit to a monomer-dimer equilibrium. Data in the presence of ligand were fit to a horizontal line. Error bars represent the standard error of the mean in the y-direction, standard deviation in x-direction.

Figure 3.3. The intracellular domain promotes ligand-independent dimerization in a concentration-dependent manner

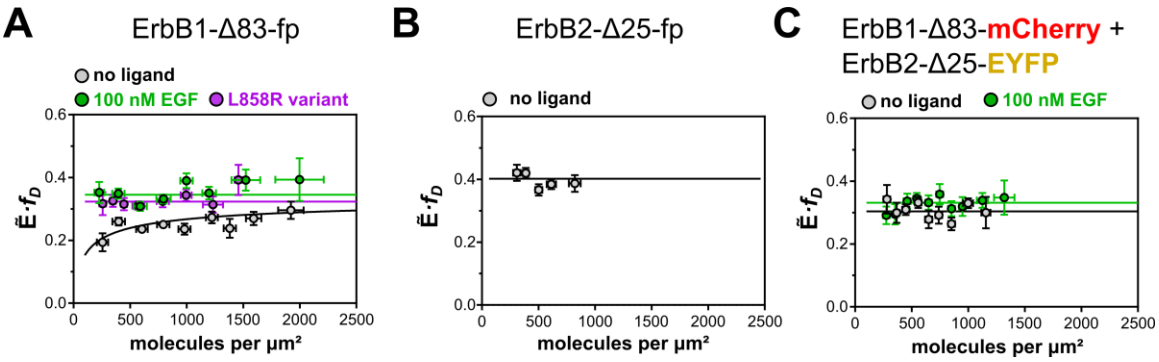

Figure 3.3. Corrected FRET efficiency as a function of total receptor membrane concentration for near full length ErbB variants. (A) ErbB1-Δ107-fp in the absence (grey circles) or presence 100 nM EGF (green circles). The L834R variant is shown in purple. The data in the absence of ligand were fit to a monomer-dimer equilibrium association model (black line). The data in the presence of ligand (green line) and for the L834R variant (purple line) were fit to a horizontal line. (B) ErbB2-Δ25-fp in the absence of EGF (grey circles), fit to a horizontal line. (C) ErbB1-Δ107-mCherry and ErbB2-Δ25-EYFP in the absence (grey circles) or presence of 100 nM EGF (green circles), both fit to a horizontal line. Error bars represent the standard error of the mean in the y-direction, standard deviation in x-direction.

Figure 3.4. Increased ErbB1 surface density promotes ligand-independent ErbB1 phosphorylation

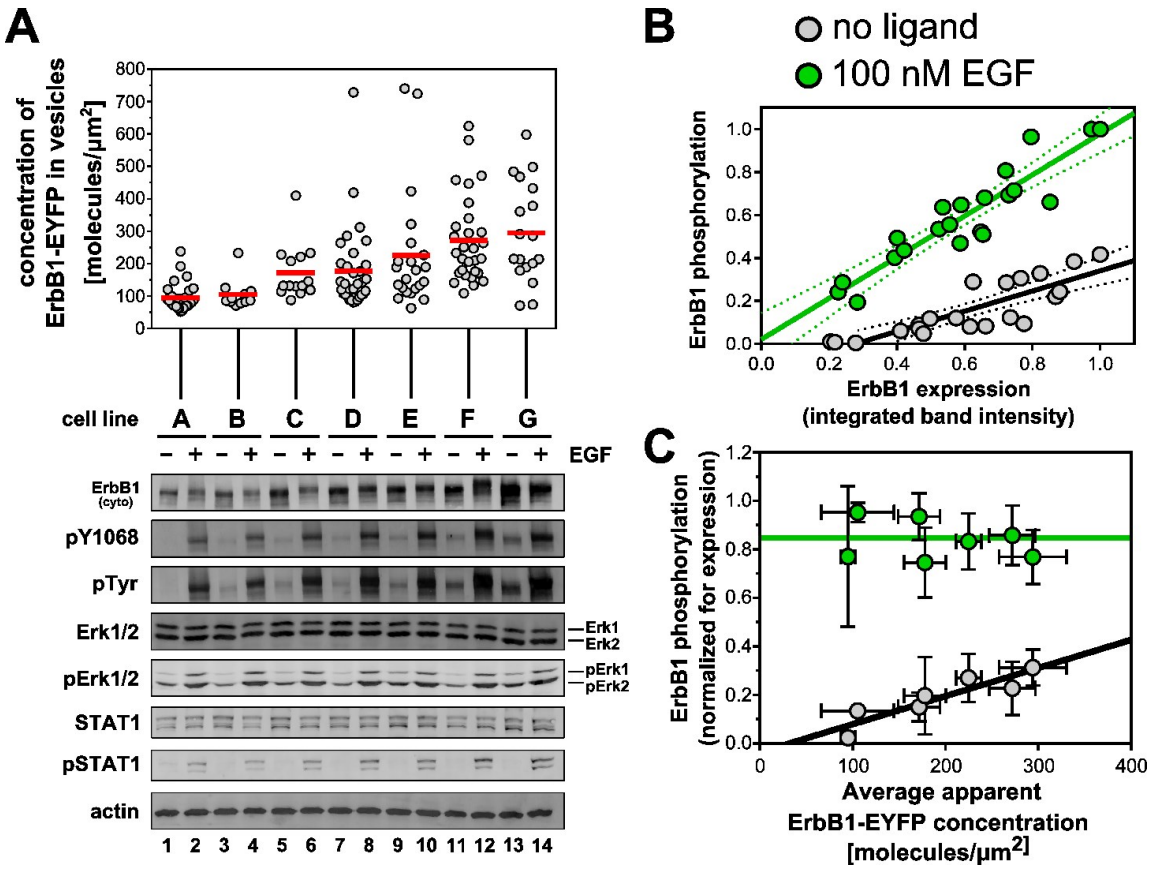

Figure 3.4. (A) Analysis of cell surface expression and ErbB1 pathway activation. Seven CHO cells stably expressing ErbB1-EYFP were treated with vesiculation buffer, and the EYFP fluorescence was measured in a confocal microscope. Each grey dot represents a measurement from a single vesicle. The red line represents the population mean. In parallel, cell lines (A-G) were cultured and treated with and without EGF, then analyzed by western blot to detect expression and phosphorylation of three proteins: ErbB1, STAT1, and Erk1/2. Cells were also blotted for actin as a loading control. Blots represent at least two independent experiments. (B) Quantification of ErbB1 phosphorylation as a function of expression level in the presence (green dots) and absence (grey dots) of EGF; *y-axis*: total relative pY1068-ErbB1 signal; *y-axis*: total relative ErbB1 receptor signal.

(C) Phosphorylation was normalized for ErbB1 expression level and grouped by cell line, plotted against the mean surface expression for each cell line from (A).

Figure 3.5. Disrupting the asymmetric dimer does not impair ligand-independent dimerization

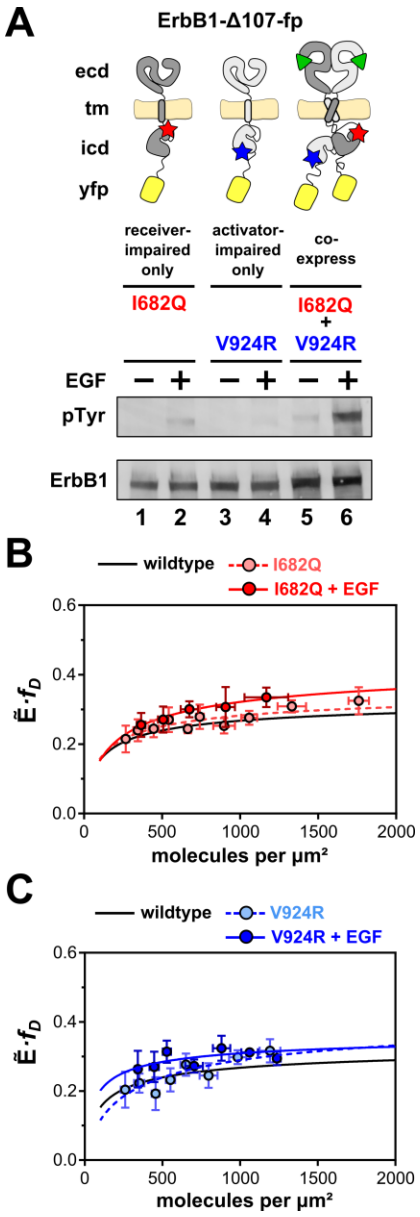

Figure 3.5. (A) Western blot analysis of ErbB1-Δ107-fp variants bearing mutations at the asymmetric dimer interface. Cartoons of each variant are shown above each blot. The I682Q and V924R mutations are indicated with red and blue stars, respectively. CHO

cells transiently expression the indicated variants were treated with or without EGF. Antibodies recognizing phosphotyrosine (4G10) and ErbB1 are indicated at the left. (B-C) QI-FRET experiments for the I682Q and V924R variants in (B) and (C), respectively. Data collected in the absence (pink, light blue) and presence (red, blue) of 100 nM EGF for the I682Q and V924R variants, respectively. The fit for wildtype ErbB1-Δ107-fp is shown as a black line for reference.

Figure 3.6. Quantitative Imaging FRET microscopy for studying ErbB proteins

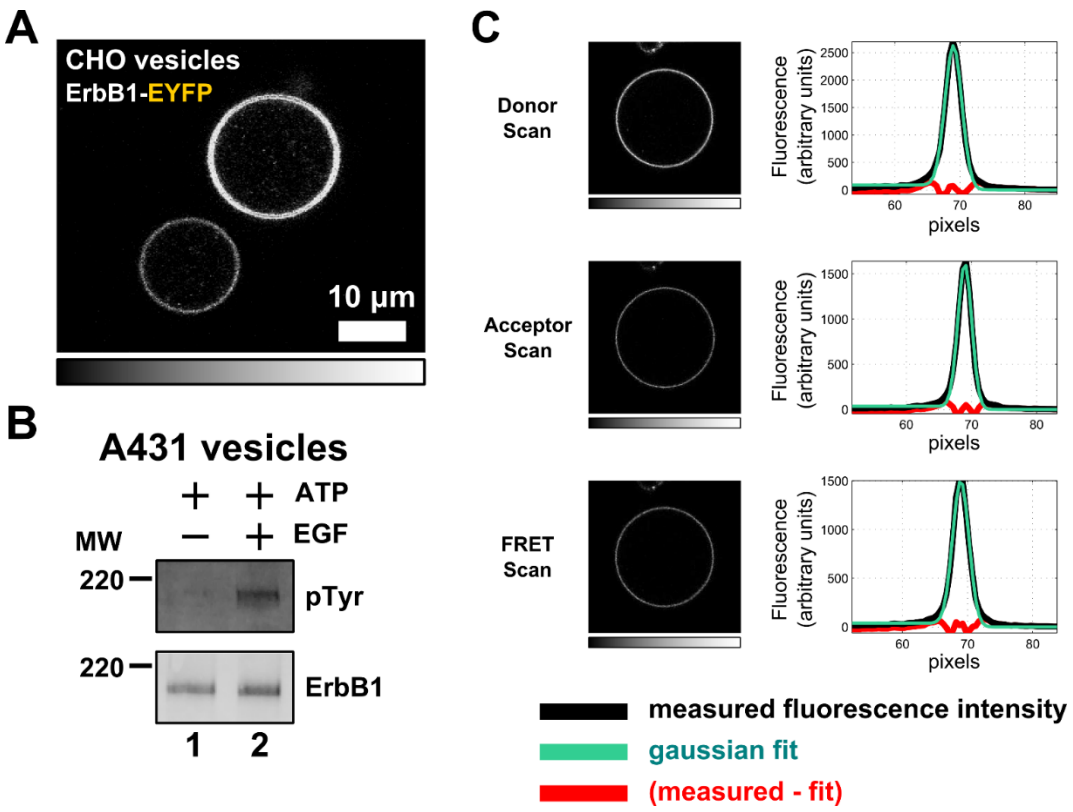

Figure 3.6. (A) Confocal image of a plasma membrane-derived vesicle produced from CHO cells expressing ErbB1-ECDTM-EYFP. Scale bar indicates 10 µm. Fluorescence intensity (arbitrary scale) indicated by the shaded bar underneath the image (black = low fluorescence, white = high). (B) A431-derived vesicles were incubated for 10 minutes with either ATP alone (lane 1) or ATP and 100 nM EGF (lane 2). Samples were separated by SDS-PAGE and analyzed by western blot to detect anti-phosphotyrosine (pTyr) and EGFR (cytoplasmic domain). Location of molecular weight standards indicated at the left of each blot. (C) Example of confocal image analysis. *Left*: Three separate confocal images taken from a single vesicle: a 'donor' scan (A), a 'FRET' scan

(B), and an ‘acceptor’ scan (see Materials and Methods). The shaded bar beneath each image denotes the relative fluorescence intensity (black = low fluorescence, white= high). *Right*: Integrated fluorescence intensity as a function of pixel number, counted from the center. Each plot shows the measured fluorescence intensity (black line), a Gaussian fit to the fluorescence intensity (turquoise line), and the difference between measured fluorescence and the fit (red line).

Figure 3.7. Enforced dimerization of the TM domains activates ErbB1

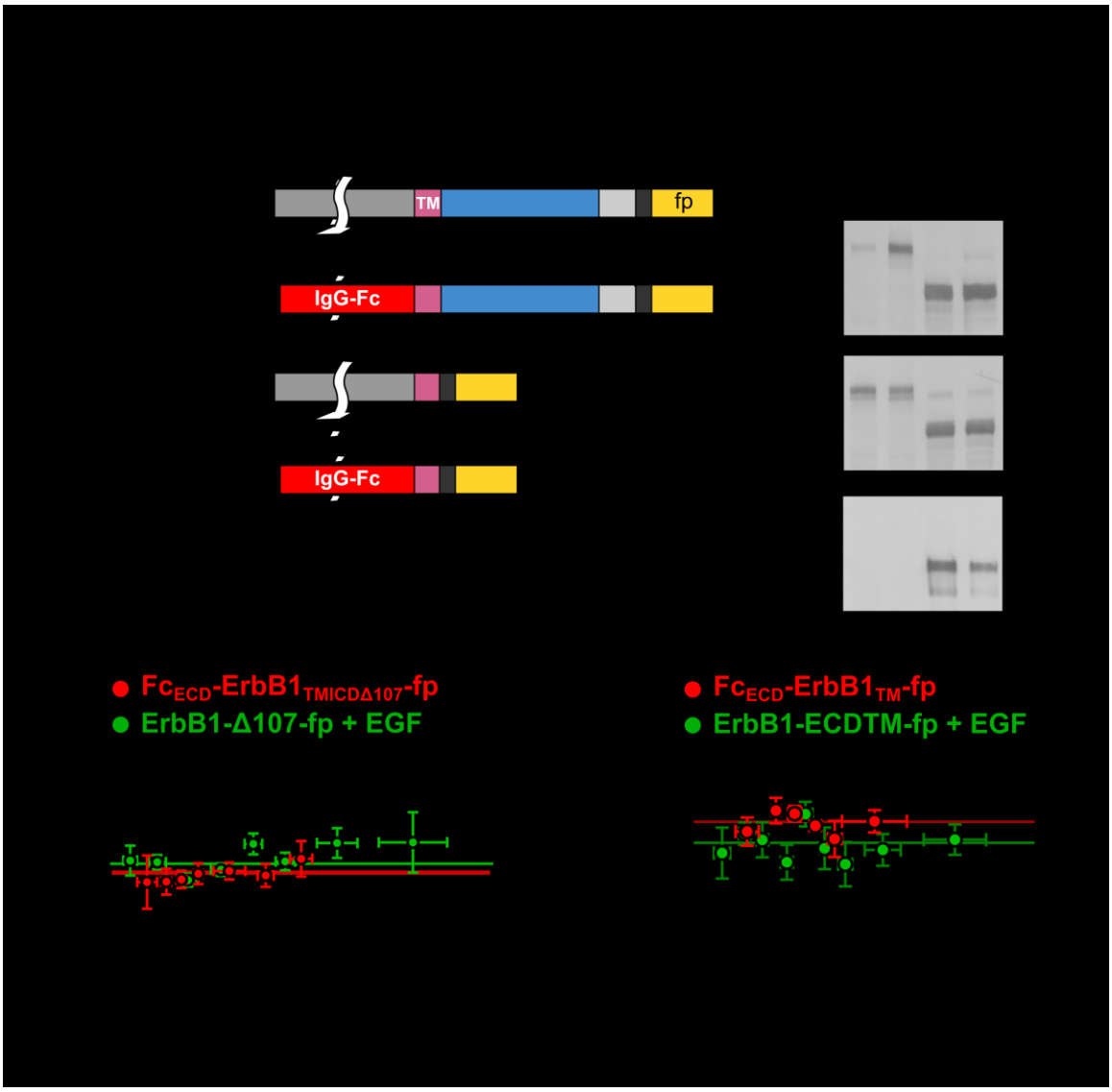

Figure 3.7. (A) Schematic of fp-tagged proteins. ErbB1-ECDTM-fp and ErbB1-Δ107-fp (identical to those shown in Figure 1A) are shown here for comparison with Fc_{ECD}-$ErbB1_{TMICD-\Delta107}$-fp and Fc_{ECD}-$ErbB1_{TM}$-fp. (B) Western blot analysis of lysates from CHO cells transiently expressing ErbB1-Δ107-fp and Fc_{ECD}-$ErbB1_{TMICD-\Delta107}$-fp. (C) FRET plot for Fc_{ECD}-$B1_{ECD-\Delta107}$-fp (red) and ErbB1-Δ107-fp in the presence (green) of

100 nM EGF. (D) FRET plot for Fc_{ECD}-$B1_{TM}$-fp (red) and ErbB1-ECDTM-fp in the absence (grey) and presence (green) of EGF.

Figure 3.8. Complex relationship between apparent cell radius and molecular surface density

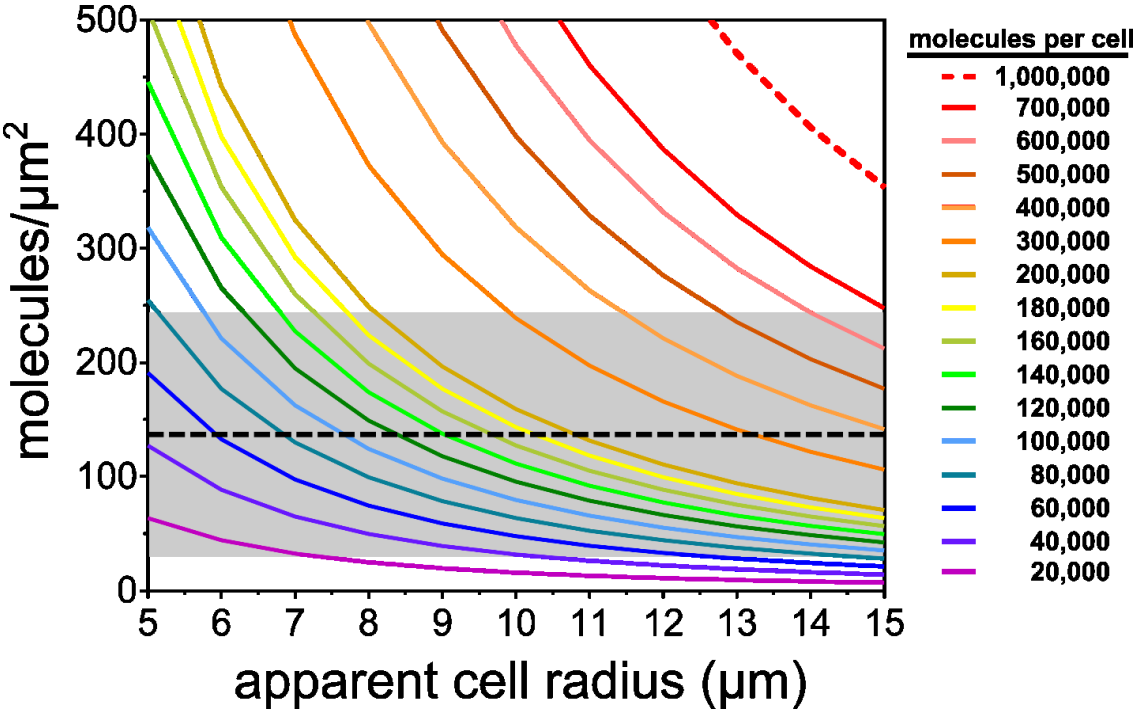

Figure 3.9. Effects of ErbB1 surface density on STAT1 expression and signaling

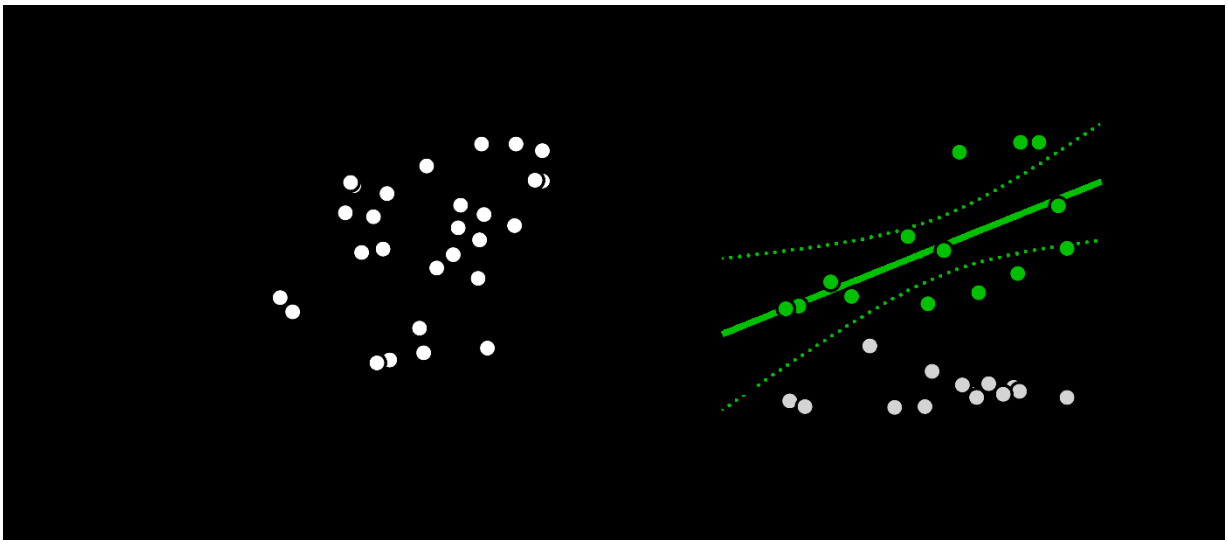

Figure 3.9. Quantification of STAT1 phosphorylation and expression as a function of ErbB1 expression. Immunoblots from Fig. 3.4 were quantified in ImageJ and plotted in panels A and B. (A) Each dot represents the average immunoblot band intensity derived from a single population of cell line. (B) STAT1 phosphorylation was divided by STAT expression and plotted on the y-axis. Data from cells treated with EGF are labeled in green, data from cells treated with no ligands are shown in grey.

Table 3.1. Measurements of ErbB1 ligand-independent association in the literature

Chapter 4. Binding of the EGF-like ligands Epigen (EPG) and Epiregulin (EPR) to ErbB1 induces partial receptor dimerization

Note to reader: This work is unpublished as of the time of submission.

Acknowledgements

Thanks to Dan Freed and Mark Lemmon for their kind gift of purified, recombinant epigen and epiregulin, and for their helpful suggestion to titrate ligand concentrations.

Abstract

The ErbB family of receptor tyrosine kinases play important roles in human health and disease. ErbBs act as regulators of a diverse set of signaling pathways within the cell, and mis-activation of the receptors can result in the progression of diseases, such as cancer. Eleven different ligands are known to bind to this family of receptors. The precise biological roles of each still remain largely unexplored, though many are thought to function as important regulators of epithelial tissue growth and development. Using quantitative FRET microscopy, we examined the ability of three ErbB ligands (EGF, epigen (EPG) and epiregulin (EPR)) to induce receptor dimerization in the membrane. EGF promotes strong ErbB1 dimer formation, whereas EPG and EPR promote partial dimer formation. These observations represent the first quantitative comparison of how

different ligands induce dimerization of ErbB1, and may help explain the unique signaling properties of these three ligands.

Introduction

Members of the epidermal growth factor (EGFR, or ErbB) family of receptor tyrosine kinases becomes activated upon binding to soluble growth factor ligands. Ligand binding to the EGFR extracellular domain (ECD) promotes the formation of activated ErbB1 dimers, which stimulates the tyrosine kinase activity within the receptor's intracellular domain (ICD). Seven growth factors are known to bind to ErbB1 in humans, and the biological functions of each ligand are known to varying degrees of certainty (Schneider & Wolf, 2009). Much of our knowledge of the ligands' functions derives from genetic experiments performed in mice. Deletion of individual ligands results in a variety of skin-related phenotypes, whereas overexpression can cause cell hyper-proliferation and is associated with tumorigenesis (Schneider & Wolf, 2009) (Schneider & Yarden, 2014).

ErbB receptors are composed of an extracellular ligand binding domain (ECD), a single transmembrane (TM) alpha helix, and an intracellular domain (ICD) which houses a tyrosine kinase. Upon activation, the kinase domains phosphorylate tyrosines located within the C-terminal end of the ICD, as well as intracellular substrates. With the exception of ErbB2, which has no known ligand, ErbB ECDs can adopt one of two conformations: a 'tethered' conformation and an 'extended' conformation (see Chapter 1, Fig. 1.1). The tethered conformation is thought to function in receptor autoinhibition,

while the extended conformation is compatible with ligand-induced, active receptor dimers. Ligand binding

The seven ErbB1 ligands (EGF, betacellulin, amphiregulin, TGF-α, heparin-binding-EGF, epiregulin, and epigen) share sequence and structural homology, and each binds to unique but overlapping subsets of ErbB receptors (Jones, et al., 1999) (Schneider & Wolf, 2009). The pairwise primary amino acid sequence identities for the soluble forms of the seven EGF-like ligands range from 29% to 53%, with most falling between 40-45%. (Figure 4.2). The reported affinities of each ligand for their receptors span several orders of magnitude, ranging from ~1 nM to >1 μM depending on the receptor-ligand interaction in question (Jones, et al., 1999). Interestingly, there does not appear to be a direct correlation between ligand-binding affinity and receptor activation. For instance, epigen (EPG) stimulates robust ErbB1 activation and cell proliferation even though EPG binds to ErbB1 with >1 μM affinity (Kochupurakkal et al., 2005). Furthermore, it is unclear how such differences in binding affinity relate to the wide range of reported phenotypes in genetic experiments.

We thus set out to investigate the effects of the binding of different ligands upon receptor dimerization. We report quantitative FRET measurements of ErbB1 dimer formation in plasma membrane-derived vesicles as a function of receptor binding to three ligands: EGF, epigen (EPG) and epiregulin (EPR). Our results provide evidence that EGF induces receptor dimerization to a greater extent than either EPR or EPG, even when differences in intrinsic ligand-binding affinity are taken into account. These

observations may explain the unique signaling properties of EPG and EPR, suggesting that EPG and EPR may act as partial agonists for ErbB1 activation.

Results

Since the different ErbB ligands possess unique receptor binding characteristics, we reasoned that they might also induce dimer formation to differing extents. To test this hypothesis, we employed QI-FRET microscopy to measure ErbB1-ECDTM-fp self-association as a function of both ligand identity and ligand concentration (Fig. 4.1.A). We observed that all three ligands (EGF, EPG, and EPR) induced dimerization of ErbB1-ECDTM-fp (Fig. 4.1), albeit to differing degrees. At saturating concentrations of EGF (0.1 μM), ErbB1-ECDTM-fp formed constitutive dimers (Fig. 4.1A), whereas both epigen (EPG) and epiregulin (EPR) induced only partial receptor dimerization, even at saturating ligand concentrations (20 μM Fig. 4.1C-D). Even at intermediate ligand concentrations (1 μM), binding to EPG and EPR induced receptor dimerization to a greater degree than was observed in the absence of ligand. Interestingly, the FRET within a receptor dimer (intrinsic FRET, $\tilde{E}$) was not significantly different between the three ligands. Thus, when compared to EGF, EPG and EPR appear to affect the receptor's homo-dimerization propensity but not the separation distance between the C-terminal ends of the TM domains within the ErbB1 dimer itself (Table 4.1).

Discussion

The differences in the reported EGF, EPG and EPR affinities for ErbB1 likely relate to their unique potentials for inducing ErbB1 dimer formation. EGF binds with 1-

10 nM affinity for the ErbB1 extracellular domain, whereas EPG and EPR bind with ~1 μm affinity (Jones, et al., 1999) (Bessman, et al., 2014) (Kochupurakkal et al., 2005). Assuming that binding of EPG and EPR to ErbB1 is saturated at 20 μm ligand concentration, this implies that binding of ErbB1 to EPR and EPG influences receptor dimerization in some other way than simple occupation of the ligand binding site on ErbB1. Ligand binding can influence receptor activity in two possible ways. First, ligand binding might alter the structural ensemble. The intrinsic FRET values for each ligand-induced dimer fall within experimental error (Table 4.1), indicating that the average separation distance between the C-terminal ends of ErbB1 does not differ significantly, though we note that our FRET assay does not report on the conformation of the ECD. Second, since ligand binding and ErbB1 dimer formation are coupled equilibria, any differences in ligand binding affinity will alter the receptor dimerization coefficients as well. It is possible that the combined effect of structural and thermodynamic perturbations produces the apparent differences in receptor dimerization observed here.

Our results further suggest that the unique signaling properties of each ligand might be ascribed to their unique potentials for inducing ErbB1 dimer formation, though the precise mechanism in which ligand binding alters this equilibrium remains has not been investigated. ErbB dimer formation certainly promotes receptor activation, but the relationship between these two phenomena remains unclear (see Chapter 3) (Bessman, et al., 2014). Ligand binding may stabilize slightly different ECD conformations; even a 1-2° change in the relative orientations of domains I and III could have large consequences

when extended to the contact regions at the ends of domains II and IV, which in turn could affect the stability of the receptor dimer. The observation that epigen induces ErbB1 dimerization to a lesser extent than EGF may explain its unique effects on ErbB1 signaling. For instance, epigen-bound receptors exhibit decreased ubiquitylation and degradation, which has been proposed to explain the apparent enhancement of signaling behavior. Monomeric receptors are less likely to become activated than dimeric ones, and might thus be less susceptible to activation-induced ubiquitylation. We note, however, that these studies were performed on truncated receptors which lacked their intracellular domains (ErbB1-ECDTM-fp). The full length ErbB1 forms ligand-independent dimers at a lower concentration threshold than the ECDTM variant. The apparent differences in dimer induction for EGF, EPR and EPG reported here should thus be viewed as qualitative indicators. Further studies using full length ErbB1 will be required in order to fully assess the differences between the three ligands.

Lastly, we note that the experiments presented here only measure receptor dimer formation. Our analysis assumes a two state system, when in reality ligand binding and ErbB1 dimerization are coupled to each other. Ligand may bind to both ErbB1 monomers and singly-liganded ErbB1 dimers, each of which may be described by a unique equilibrium constant. In the same way, both liganded and unliganded ErbB1 dimers may exhibit unique dimerization coefficients. A full understanding of the relationship between the two processes requires parallel observation of ErbB1 dimer formation as well as ligand binding (Macdonald & Pike, 2008). The trends observed here should therefore be interpreted as qualitative indicators of receptor dimer formation.

Figure 4.1. Epigen and epiregulin induce partial ErbB1 dimerization

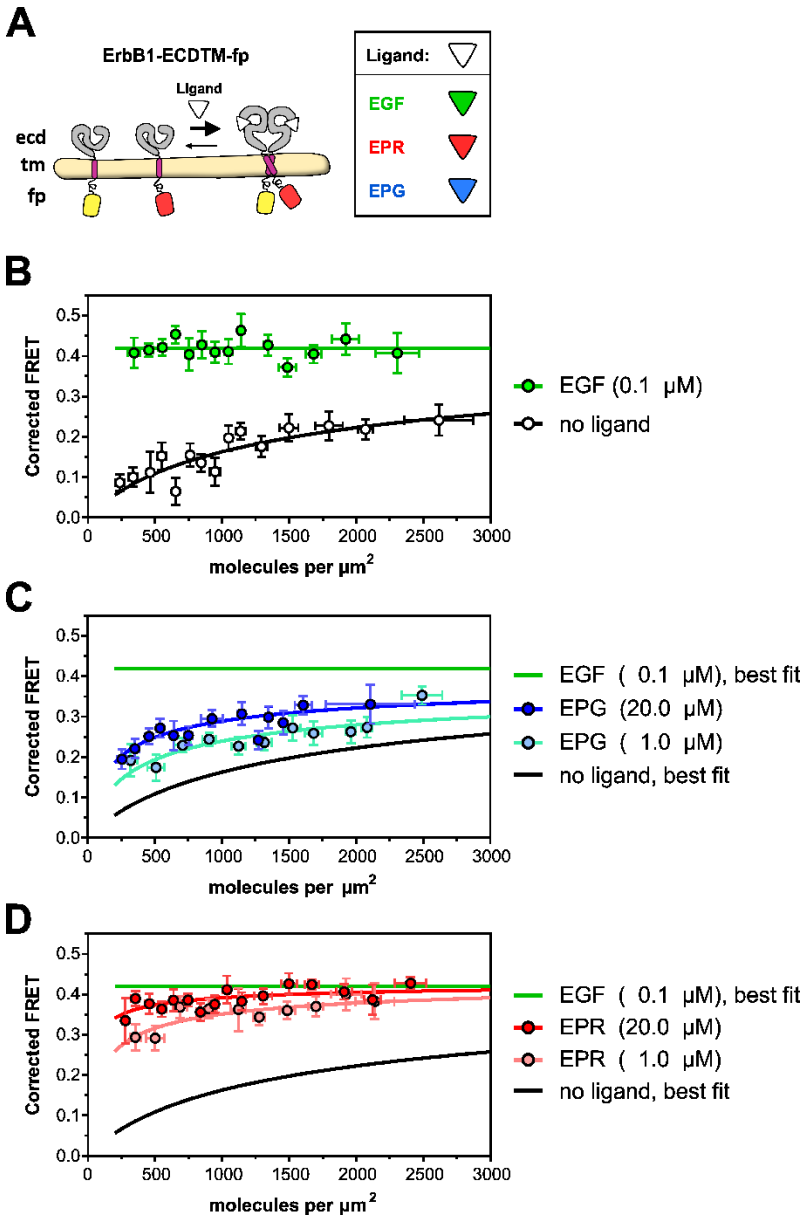

Figure 4.1. Corrected FRET as a function of concentration, measured from CHO cell vesicles expressing. (A) Schematic of ErbB1-ECDTM-fp constructs used in (B-D). Vesicles were incubated with either no ligand, EGF, epigen (EPG) or epiregulin (EPR). (B) ErbB1-ECDTM-fp dimerization in the absence (unfilled circles) and presence (green

circles) of 0.1 μM EGF. Lines indicate the best fit to the dimerization model. (C-D) Comparison of ligand-independent, EGF-induced, EPG-induced, and EPR-induced dimerization. (C) EPG was assayed at 20 μM (royal blue) and 1 μM (light blue). (D) EPG was assayed at 20 μM (royal blue) and 1 μM (light blue). In C-D, the best fit for ligand-independent (black line) and EGF-dependent (green line) dimerization are included for comparison.

Figure 4.2. Primary sequence analysis of the seven EGF-like ligands

A

```
EGF       -NSDSECPLSHDGYCLHDGVCMYIEALDKYACNCVVGYIGERCQYRDLKWWELR
BTC       -GHFSRCPKQYKHYCIK-GRCRFVVAEQTPSCVCDEGYIGARCERVDLFYLRGD
TGF-α     -SHFNDCPDSHTQFCFH-GTCRFLVQEDKPACVCHSGYVGARCEHADLLAVVAA
AREG      -KKKNPCNAEFQNFCIH-GECKYIEHLEAVTCKCQQEYFGERCGEKSMKTHSMI
HB-EGF    -KKRDPCLRKYKDFCIH-GECKYVKELRAPSCICHPGYHGERCHGLSLPVENRL
EPR       QVSITKCSSDMNGYCLH-GQCIYLVDMSQNYCRCEVGYTGVRCEHFFLTVHQPL
EPG       -KFSHLCLEDHNSYCIN-GACAFHHELEKAICRCFTGYTGERCEHLTLTSYAVD
```

B Sequence Identity Matrix

	EGF	AREG	BTC	EPG	EPR	HB-EGF	TGF-α
EGF	100.0%						
AREG	39.5%	100.0%					
BTC	40.9%	30.6%	100.0%				
EPG	40.5%	30.4%	39.0%	100.0%			
EPR	41.9%	29.5%	34.8%	47.6%	100.0%		
HB-EGF	40.5%	44.2%	43.9%	43.9%	34.0%	100.0%	
TGF-α	45.5%	34.2%	53.3%	41.3%	42.1%	39.0%	100.0%

0% 50% 100%

C Sequence Similarity Matrix

	EGF	AREG	BTC	EPG	EPR	HB-EGF	TGF-α
EGF	100.0%						
AREG	51.2%	100.0%					
BTC	54.5%	61.1%	100.0%				
EPG	57.1%	56.5%	48.8%	100.0%			
EPR	62.8%	54.5%	52.2%	61.9%	100.0%		
HB-EGF	56.8%	67.3%	63.4%	56.1%	46.8%	100.0%	
TGF-α	63.6%	44.7%	66.7%	54.3%	50.0%	56.1%	100.0%

0% 50% 100%

Figure 4.2. (A) Multiple sequence alignment from the MUSCLE server (http://www.ebi.ac.uk/Tools/msa/muscle/). The sequences represent the soluble EGF-like domains of the mature growth factor proteins. (B-C) Pairwise sequence alignments were performed using the EMBOSS server (http://www.ebi.ac.uk/Tools/psa/emboss_water/). The identity/similarity matrices are colored according to the degree of identity/similarity, with green indicating 0%, yellow indicating 50% and red indicating 100%. Abbreviations: EGF, epidermal growth factor; AREG, amphiregulin; BTC, betacellulin; EPG, epigen; EPR, epiregulin; HB-EGF, heparin-binding EGF; TGF-α, transforming growth factor alpha.

Table 4.1. Table of best fit parameters to a monomer-dimer equilibrium

Ligand	Concentration	K_{app} (molecules per µm²)	Intrinsic FRET ($\tilde{E}$)
EGF	0.1 µM	constitutive dimer	0.42 ± 0.03
Epiregulin	20 µM	26 ± 23	0.44 ± 0.03
Epiregulin	1 µM	132 ± 109	0.45 ± 0.05
Epigen	20 µM	275 ± 133	0.44 ± 0.03
Epigen	1 µM	591 ± 314	0.41 ± 0.05

Table 4.1. The data in figure 4.1 were fit to the monomer dimer equilibrium described in Chapter 3 (see *Materials and Methods*). The best fit parameters (K_{app} and Intrinsic FRET, +/- standard error) are indicated for each ligand condition.

References

Accili, et al.,, D., 1996. Early neonatal death in mice homozygous for a null allele of the insulin receptor gene. *Nature Genetics,* pp. 12:106-9.

Alvarado, D., Klein, D. & Lemmon, M., 2010. Structural basis for negative cooperativity in growth factor binding to an EGF receptor. *Cell,* p. 142:568–579.

Arkhipov, et al., A., 2013. Architecture and membrane interactions of the EGF receptor. *Cell,* pp. 152:557-569.

Avraham, R. & Yarden, Y., 2011. Feedback regulation of EGFR signalling: decision making by early and delayed loops. *Nat Rev Mol Cell Biol,* pp. 12:104-17.

Baer, et al.,, K., 2001. Dimerization-induced activation of soluble insulin/IGF-1 receptor kinases: an alternative mechanism of activation. *Biochemistry,* pp. 40:14268-14278.

Bass, J., Kurose, T., Pashmforoush, M. & Steiner, D., 1996. Fusion of insulin receptor ectodomains to immunoglobulin constant domains reproduces high-affinity insulin binding in vitro. *The Journal of Biological Chemistry,* pp. 271:19367-19375.

Bessman, N., Bagchi, A., Ferguson, K. & Lemmon, M., 2014. Complex relationship between ligand binding and dimerization in the epidermal growth factor receptor. *Cell Reports,* pp. 9:1306-17.

Boerner, J., McManus, M., Martin, G. & Maihle, N., 2000. Ras-independent oncogenic transformation by an EGF-receptor mutant. *J Cell Sci. ,* pp. 113:935-42.

Bouyain, S. et al., 2005. The extracellular region of ErbB4 adopts a tethered conformation in the absence of ligand. *Proc Natl Acad Sci USA,* p. 102:15024–15029.

Burgess, A., 2003. An open-and-shut case? Recent insights into the activation of EGF/ErbB receptors. *Mol Cell.,* p. 12:541–552.

Burgess, A., 2008. Structure physiology signalling and therapeutic targets. *Growth Factors,* p. 26:263–274.

Cao, H. et al., 1992. An extra cysteine proximal to the transmembrane domain induces differential cross-linking of p185neu and p185neu. *The Journal of Biological Chemistry,* pp. 267:20489-20492.

Cheatham, B. et al., 1993. Substitution of the erbB-2 oncoprotein transmembrance domain activates the insulin receptor and modulates the action of insulin and insulin-receptor substrate 1. *Proceedings of the National Academy of Sciences of USA,* pp. 90:7336-7340.

Chen, L. et al., 2010a. Measuring the energetics of membrane protein dimerization in mammalian membranes. *Journal of the American Chemical Society,* pp. 132:3628-3635.

Chen, L., Placone, J., Novicky, L. & Hristova, K., 2010b. The extracellular domain of fibroblast growth factor receptor 3 inhibits ligand-independent dimerization. *Science Signaling,* p. 3:ra86.

Cho, et al., H., 2003. Structure of the extracellular region of HER2 alone and in complex with the Herceptin Fab. *Nature,* p. 421:756–760.

Cho, H. & Leahy, D., 2002. Structure of the extracellular region of HER3 reveals an interdomain tether. *Science,* p. 297:1330–1333.

Chung, et al., I., 2010. Spatial control of EGF receptor activation by reversible dimerization on living cells. *Nature,* p. 464(7289):783–787.

Coskun, U., Grzybek, M., Dreschel, D. & Simons, K., 2011. Regulation of human EGF receptor by lipids. *Proc Natl Acad Sci U S A,* pp. 108:9044-8.

De Meyts, P., 2004. Insulin and its receptor: structure, function and evolution. *Bioessays,* pp. 26:1351-1362.

De Meyts, P. & Whittaker, J., 2002. Structural biology of insulin and IGF1 receptors: implications for drug design. *Nature Reviews Drug Discovery,* pp. 1:769-783.

Del Piccolo, N. et al., 2012. Production of plasma membrane vesicles with chloride salts and their utility as a cell membrane mimetic for biophysical characterization of membrane protein interactions. *Analytical Chemistry,* pp. 84:8650-8655.

Ekstrand et al., A., 1991. Genes for epidermal growth factor receptor, transforming growth factor alpha, and epidermal growth factor and their expression in human gliomas in vivo. *Cancer Research,* pp. 51:2164-72.

Endres, et al., N., 2013. Conformational coupling across the plasma membrane in activation of the EGF receptor. *Cell,* pp. 152:543-556.

Endres, N., Barros, T., Cantor, A. & Kuriyan, J., 2014. Emerging concepts in the regulation of the EGF receptor and other receptor tyrosine kinases. *Trends Biochem Sci,* pp. 39:437-46.

Ferguson, et al., K., 2003. EGF activates its receptor by removing interactions that autoinhibit ectodomain dimerization. *Mol Cell.,* p. 11:507–517.

Finger, C., Escher, C. & Schneider, D., 2009. The single transmembrane domains of human receptor tyrosine kinases encode self-interactions. *Sci Signal.,* p. 2:ra56.

Fratalli, A., Treadway, J. & Pessin, J., 1991. Evidence supporting a passive role for the insulin receptor transmembrane domain in insulin-dependent signal transduction. *The Journal of Biological Chemistry,* pp. 266:9829-9834.

Frattali, A., Treadway, J. & Pessin, J., 1992. Transmembrane signaling by the human insulin receptor kinase. Relationship between intramolecular beta subunit trans- and cis-autophosphorylation and substrate kinase activation. *The Journal of Biological Chemistry,* pp. 267:19521-19528.

Freed, D., Alvarado, D. & Lemmon, M., 2015. Ligand regulation of a constitutively dimeric EGF receptor. *Nat Commun,* p. 6:7380.

Gadella, T. J. & Jovin, T., 1995. Oligomerization of epidermal growth factor receptors on A431 cells studied by time-resolved fluorescence imaging microscopy. A stereochemical model for tyrosine kinase receptor activation.. *J Cell Biol.,* p. 129:1543–1558.

Garrett, et al., T., 2003. The crystal structure of a truncated ErbB2 ectodomain reveals an active conformation, poised to interact with other ErbB receptors. *Mol Cell,* p. 11:495–505.

Groves, J. & Kuriyan, J., 2010. Molecular mechanisms in signal transduction at the membrane. *Nat Struct Mol Biol,* pp. 17:659-65.

Heldin, C., 1995. Dimerization of cell surface receptors in signal transduction. *Cell,* p. 80:213–223.

Houde, D. & Demarest, S., 2011. Fine details of IGF-1R activation, inhibition, and asymmetry determined by associated hydrogen /deuterium-exchange and peptide mass mapping. *Structure,* pp. 19,:90-900.

Hoyne, e. a. P., 2000. High affinity insulin binding by soluble insulin receptor extracellular domain fused to a leucine zipper. *FEBS Letters,* pp. 479:15-18.

Jones, J., Akita, R. & SLiwkowski, M., 1999. Binding specificities and affinities of egf domains for ErbB receptors. *FEBS Letters,* pp. 447:227-31.

Jura, e. a. N., 2009. Mechanism for activation of the EGF receptor catalytic domain by the juxtamembrane segment. *Cell,* pp. 137:1293-1307.

Kavran, J. et al., 2014. How IGF-1 activates its receptor. *eLife,* p. 3:e03772.

King, C. et al., 2014. The FRET signatures of noninteracting proteins in membranes: simulations and experiments. *Biophysical Journal,* pp. 106:1-9 .

King, C., Stoneman, M., Raicu, V. & Hristova, K., 2016. Fully quantified spectral imaging reveals in vivo membrane protein interactions. *Integ Biol (Camb),* pp. 8:216-29.

Kleiman, e. a. L., 2011. Rapid phospho-turnover by receptor tyrosine kinases impacts downstream signaling and drug binding. *Molecular Cell,* pp. 43:723-737.

Kochupurakkal et al., B., 2005. Epigen, the last ligand of ErbB receptors, reveals intricate relationships between affinity and mitogenicity. *J Biol Chem,* pp. 280:8503-12.

Kovacs, E. et al., 2015. Analysis of the Role of the C-Terminal Tail in the Regulation of the Epidermal Growth Factor Receptor. *Mol Cell Biol,* pp. 35:3038-102.

Lahusen, T. et al., 2007. Epidermal growth factor receptor tyrosine phosphorylation and signaling controlled by a nuclear receptor coactivator, amplified in breast cancer 1. *Cancer Research,* p. 67:7256.

Lakowicz, J., 2006. *Principles of Fluorescence Spectroscopy.* 3rd ed. ed. s.l.:s.n.

Leahy, D. et al., 2000. A mammalian expression vector for expression and purification of secreted proteins for structural studies. *Protein Expr Purif.,* p. 20:500–506.

Lee, et al., S., 2015. Inhibition of ErbB3 by a monoclonal antibody that locks the extracellular domain in an inactive configuration.. *Proc Natl Acad Sci U S A. ,* pp. 112:13225-30.

Lee, J., Miyazaki, M., Romeo, G. & Shoelson, S., 2014. Insulin receptor activation with transmembrane domain ligands. *The Journal of Biological Chemistry,,* pp. 289:19769-19777.

Lemmon, M., 2009. Ligand-induced ErbB receptor dimerization. *Exp Cell Res,* p. 315:638–648.

Lemmon, M. et al., 1997. Two EGF molecules contribute additively to stabilization of the EGFR dimer.. *EMBO Journal,* pp. 16:281-94.

Lemmon, M. & Schlessinger, J., 2010. Cell signaling by receptor tyrosine kinases. *Cell,* pp. 141:1117-1134.

Lew, E., Furdui, C., Anderson, K. & Schlessinger, J., 2009. The precise sequence of FGF receptor autophosphorylation is kinetically driven and is disrupted by oncogenic mutations. *Science SIgnaling,* p. 2:ra6.

Li, E., Placone, J., Merzlyakov, M. & Hristova, K., 2008. Quantitative measurements of protein interactions in a crowded cellular environment. *Analytical Chemistry,* pp. 80:5976-5985.

Lin, et al., W., 2014. H-Ras forms dimers on membrane surfaces via a protein-protein interface. *Proc Natl Acad Sci U S A.,* pp. 111:2996-3001.

Liu, et al., P., 2007. Investigation of the dimerization of proteins from the epidermal growth factor receptor family by single wavelength fluorescence cross-correlation spectroscopy. *Biophys J.,* pp. 93:684-98.

Liu, J. et al., 1993. Mice carrying null mutations of the genes encoding insulin-like growth factor I (Igf-1) and type 1 IGF receptor (Igf1r). *Cell,* pp. 75:59-72.

Liu, P. et al., 2012. A single ligand is sufficient to activate EGFR dimers. *Proc. Natl. Acad. Sci. USA,* pp. 109:10861-10866.

Lu, C. e. a., 2010. Structural evidence for loose linkage between ligand binding and kinase activation in the epidermal growth factor receptor. *Mol Cell Biol,* p. 30:5432–5443.

Macdonald, J. & Pike, L., 2008. Heterogeneity in EGF-binding affinities arises from negative cooperativity in an aggregating system. *Proc Natl Acad Sci USA.,* p. 105:112–117..

Macdonald-Obermann, J., Piwinica-Worms, D. & Pike, L., 2012. Mechanics of EGF receptor/ErbB2 kinase activation revealed by luciferase fragment complementation imaging. *Proc Natl Acad Sci USA,* p. 109:137–142.

Maruyama, 2015. Activation of transmembrane cell-surface receptors via a common mechanism? The "rotation model". *Bioessays,* pp. 37:959-67.

Mattoon, D. et al., 2004. The tethered configuration of the EGF receptor extracellular domain exerts only a limited control of receptor function. *Proc Natl Acad Sci USA,* p. 101:923–928.

McKern et al., N., 2006. Structure of the insulin receptor ectodomain reveals a folded-over conformation. *Nature,* pp. 443:218-21.

McManus, M., Lingle, W., Salisbury, J. & Maihle, N., 1997. A transformation-associated complex involving tyrosine kinase signal adapter proteins and caldesmon links v-erbB signaling to actin stress fiber disassembly. *Proc Natl Acad Sci U S A. ,* pp. 94:11351-6.

Mendrola, J., Berger, M., King, M. & Lemmon, M., 2002. The single transmembrane domains of ErbB receptors self-associate in cell membranes. *J Biol Chem,* pp. 277:4704-12.

Menting, et al., J., 2013. How insulin engages its primary binding site on the insulin receptor. *Nature,* pp. 493:241-245.

Mi, L. et al., 2011. Simultaneous visualization of the extracellular and cytoplasmic domains of the epidermal growth factor receptor. *Nat Struct Mol Biol,* pp. 18:984-9.

Moriki, T., Maruyama, H. & Maruyama, I., 2001. Activation of preformed EGF receptor dimers by ligand-induced rotation of the transmembrane domain. *J Mol Biol.,* p. 311:1011–1026.

Mynarcik, D., Yu, G. & Whittaker, J., 1996. Alanine-scanning mutagenesis of a C-terminal ligand binding domain of the insulin receptor alpha subunit. *The Journal of Biological Chemistry,* pp. 271:2439-2442.

Nagy, P., Claus, J., Jovin, T. & Arndt-Jovin, D., 2010. Distribution of resting and ligand-bound ErbB1 and ErbB2 receptor tyrosine kinases in living cells using number and brightness analysis. *Proc Natl Acad Sci U S A. ,* pp. 10716524-9.

Pines, G. et al., 2010. EGFRvIV: a previously uncharacterized oncogenic mutant reveals a kinase autoinhibitory mechanism. *Oncogene,* pp. 29:5850-60.

Pollak, M., 2012. The insulin and insulin-like growth factor receptor family in neoplasia: an update. *Nature Reviews Cancer,* pp. 12:159-169.

Qiu, et al., C., 2009. In vitro enzymatic characterization of near full length EGFR in activated and inhibited states. *Biochemistry,* p. 48:6624–6632.

Raicu, et al., V., 2008. Determination of supramolecular structure and spatial distribution of protein complexes in living cells. *Nature Photonics,* pp. 3:107-113.

Reddy, R. et al., 2016. Early signaling dynamics of the epidermal growth factor receptor. *Proc Natl Acad Sci U S A. ,* pp. 113:3114-9.

Reidel, H., Dull, T., Schlessinger, J. & Ullrich, A., 1986. A chimaeric receptor allows insulin to stimulate tyrosine kinase activity of epidermal growth factor receptor. *Nature,* pp. 324:68-70.

Russ, W. & Engelman, D., 2000. The GxxxG motif: a framework for transmembrane helix-helix association. *Journal of Molecular Biology, ,* pp. 296:911-919.

Saffarian, S., Li, Y., Elson, E. & Pike, L., 2007. Oligomerization of the EGF receptor investigated by live cell fluorescence intensity distribution analysis. *Biophys J,* pp. 93:1021-31.

Sako, Y., Minoghchi, S. & Yanagida, T., 2000. Single-molecule imaging of EGFR signalling on the surface of living cells. *Nat Cell Biol.,* p. 2:168–172.

Sarabipour, et al., 2015. Analytical characterization of plasma membrane-derived vesicles produced via osmotic and chemical vesiculation. *Biochim Biophys Acta,* pp. 1848:1591-8.

Schaffer, L., 1994. A model for insulin binding to the insulin receptor. *European Journal of Biochemistry,* pp. 221:1127-1132.

Schaffer, L. & Ljungqvist, L., 1992. Identification of a disulfide bridge connecting the alpha-subunits of the extracellular domain of the insulin receptor. *Biochemical and Biophysical Research Communications,* pp. 189:650-653.

Schneider, M. & Wolf, E., 2009. The epidermal growth factor receptor ligands at a glance. *J Cell Physiol,* pp. 218:460-6.

Schneider, M. & Yarden, Y., 2014. Structure and function of epigen, the last EGFR ligand. *Semin Cell Dev Biol,* pp. 28:57-61.

Shan et al., Y., 2012. Oncogenic mutations counteract intrinsic disorder in the EGFR kinase and promote receptor dimerization.. *Cell,* pp. 149:860-70.

Shoelson, S., White, M. & Kahn, C., 1988. Tryptic activation of the insulin receptor. Proteolytic truncation of the alpha-subunit releases the beta-subunit from inhibitory control. *The Journal of Biological Chemistry,* pp. 263:4852-4860.

Siddle, K., 2011. Signalling by insulin and IGF receptors: supporting acts and new players. *Journal of Molecular Endocrinology,* pp. 47:R1-R10.

Siddle, K., 2012. Molecular basis of signaling specificity of insulin and IGF receptors: neglected corners and recent advances. *Frontiers in Endocrinology,* p. 3:34.

Slamon et al., D., 1989. Studies of the HER-2/neu proto-oncogene in human breast and ovarian cancer.. *Science,* pp. 244:707-12.

Smith, et al., B., 2010. Structural resolution of a tandem hormone-binding element in the insulin receptor and its implications for design of peptide agonists. *Proceedings of the National Academy of Sciences of USA,* pp. 107:6771-6776 .

Sparrow, L. et al., 1997. The disulfide bonds in the C-terminal domains of the human insulin receptor ectodomain. *The Journal of Biological Chemistry,* pp. 272:29460-29467.

Stanley, A. & Fleming, K., 2005. The transmembrane domains of ErbB receptors do not dimerize strongly in micelles. *J Mol Biol.,* pp. 347:759-72.

Tamura, S., Fukita-Yamaguchi, Y. & Larner, J., 1983. Insulin-like effect of trypsin on the phosphorylation of rat adipocyte insulin receptor. *The Journal of Biological Chemistry,* pp. 258:14749-14752.

Ullrich, et al.,, A., 1985. Nature. *Human insulin receptor and its relationship to the tyrosine kinase family of oncogenes,* pp. 313:756-761.

Valley et al., C., 2015. Enhanced dimerization drives ligand-independent activity of mutant epidermal growth factor receptor in lung cancer. *Mol Biol Cell,* pp. 26:4087-99.

Walker, et al., F., 2004. CR1/CR2 interactions modulate the functions of the cell surface epidermal growth factor receptor. *J Biol Chem,* p. 279:22387–22398.

Ward, C., Menting, J. & Lawrence, M., 2013. The insulin receptor changes conformation in unforeseen ways on ligand binding: sharpening the picture of insulin receptor activation. *Bioessays,* pp. 35:945-954.

Whittaker, L, Hao, C., Fu, W. & Whittaker, J., 2008. High-affinity insulin binding: insulin interacts with two receptor ligand binding sites. *Biochemistry,* pp. 47:12900-12909.

Whittaker, J. et al., 2001. Alanine scanning mutagenesis of a type 1 insulin-like growth factor receptor ligand binding site. *The Journal of Biological Chemistry,* pp. 276:43980-43986.

Williams, P., Mynarcik, D., Yu, G. & Whittaker, J., 1995. Mapping of an NH2-terminal ligand binding site of the insulin receptor by alanine scanning mutagenesis. *The Journal of Biological Chemistry,* pp. 270:3012-3016.

Wu et al., J., 2008. Small-molecule inhibition and activation-loop trans-phosphorylation of the IGF1 receptor. *The EMBO Journal,* pp. 27:1985-1994.

Yamada, K., Goncalves, E., Kahn, C. & Shoelson, S., 1992. Substitution of the insulin receptor transmembrane domain with the c-neu/erbB2 transmembrane domain constitutively activates the insulin receptor kinase in vitro. *The Journal of Biological Chemistry,* pp. 267:12452-1246.

Yarden, Y. & Schlessinger, J., 1987. Epidermal growth factor induces rapid, reversible aggregation of the purified epidermal growth factor receptor. *Biochemistry,* p. 26:1443–1451.

Yu, X. et al., 2002. Ligand-independent dimer formation of epidermal growth factor receptor (EGFR) is a step separable from ligand-induced EGFR signaling. *Mol Cell Biol,* pp. 13:2547-57.

Zacharias, D., Violin, D., Newton, A. & Tsien, R., 2002. Partitioning of lipid-modified monomeric GFPs into membrane microdomains of live cells.. *Science,* pp. 296:913-6.

Zhang, X. et al., 2006. An allosteric mechanism for activation of the kinase domain of epidermal growth factor receptor. *Cell,* pp. 125:1137-1149.

Zhang, X. et al., 2010. Structural basis for negative cooperativity in growth factor binding to an EGF receptor. *Cell,* p. 142:568–579.

Zhang, X. et al., 2007. Inhibition of the EGF receptor by binding of MIG6 to an activating kinase domain interface.. *Nature,* pp. 450:741-4.

Curriculum Vitae

Patrick O. Byrne

pbyrne3@jhu.edu

725 North Wolfe Street
Hunterian 713
Department of Biophysics and Biophysical Chemistry
Johns Hopkins University, School of Medicine
Baltimore, MD, 21205

BIRTH

Philadelphia, Pennsylvania
1987

EDUCATION

Pennsylvania State University — University Park, PA
B.S. Chemistry, with honors in Biochemistry and Molecular Biology. — 2010
Dissertation: Differential and inducible expression of yellow fluorescent protein in the marine cyanobacterium *Synechococcus* sp. PCC 7002

Johns Hopkins University — Baltimore, MD
Ph. D. (in progress), Molecular Biophysics. — 2016 (expected)

GRANTS AND AWARDS

National Science Foundation Graduate Research Fellowship, Honorable Mention — 2012

RESEARCH EXPERIENCE

Bryant Laboratory — 2008-2010
Pennsylvania State University
Department of Biochemistry and Molecular Biology

- Helped design and develop a plasmid for expressing non-native proteins in cyanobacteria
- Engineered a strain of cyanobacteria which expressed non-native proteins at tunable levels using a CO_2-inducible promoter

Leahy Laboratory — 2010-present
Johns Hopkins University, School of Medicine
Department of Biophysics and Biophysical Chemistry

- worked in collaboration with the Hristova Laboratory (Johns Hopkins University)

- Employed FRET methods developed with the Hristova laboratory to investigate the molecular mechanisms governing receptor tyrosine kinase activation and autoinhibition

CONFERENCE PRESENTATIONS

Byrne PO, Hristova K, Leahy DJ. (2015). Mechanisms of dimerization and autoinhibition in the EGF receptor family. *Biophysical Journal*, Abstracts Issue, Vol. 108, Issue 2, p351a.

- Oral Presentation for the "Membrane Receptors and Signal Transduction" platform at the 59th Biophysical Society Meeting, Baltimore, MD, February 2015.
- Poster Presentation "FRET Studies of EGF receptor activation" at the 60th meeting of the Biophysical Society, Los Angeles, CA February 2016.

PROFESSIONAL ASSOCIATIONS

Member, Biophysical Society 2010-present

TEACHING EXPERIENCE

Teaching Assistant 2008-2010
Pennsylvania State University, Department of Biology

- Three courses total, one per year: Introductory Biology (2008), Molecular and Cellular Biology (2009), and Biology for Non-Majors (2010)
- For each course, managed weekly laboratory classes of 20-30 students and held recitation and review sessions covering course material

PUBLICATIONS

1. Kavran JM, McCabe JM, **Byrne PO**, Connacher MK, Wang Z, Ramek A, Sarabipour S, Shan Y, Shaw DE, Hristova K, Cole PA, Leahy D. "How IGF1 Activates its Receptor." *eLife* 2014;10.7554/eLife.03772
2. King C, Sarabipour S, **Byrne P**, Leahy DJ, Hristova K. "The FRET signatures of noninteracting proteins in membranes: simulations and experiments." *Biophys. J.* 2014;106(6), 1309-17
3. Liu P, Cleveland TE 4th, Bouyain S, **Byrne PO**, Longo PA, Leahy DJ. "A single ligand is sufficient to activate EGFR dimers." *Proc. Natl. Acad. Sci USA* 2012, 109(27):10861-6.
4. Xu Y, Alvey RM, **Byrne PO**, Graham JE, Shen G, Bryant DA. "Expression of genes in cyanobacteria: adaptation of endogenous plasmids as platforms for high-level gene expression in Synechococcus sp. PCC 7002." *Methods Mol Biol*. 2011;684:273-93.
5. Byrne, P.O. (2010) Undergraduate Thesis. "Differential and inducible expression of yellow fluorescent protein in the marine cyanobacterium Synechococcus sp. PCC 7002".

Pennsylvania State University Press. Available online at:
http://honors.libraries.psu.edu/theses/approved/WorldWideIndex/EHT-465/index.html